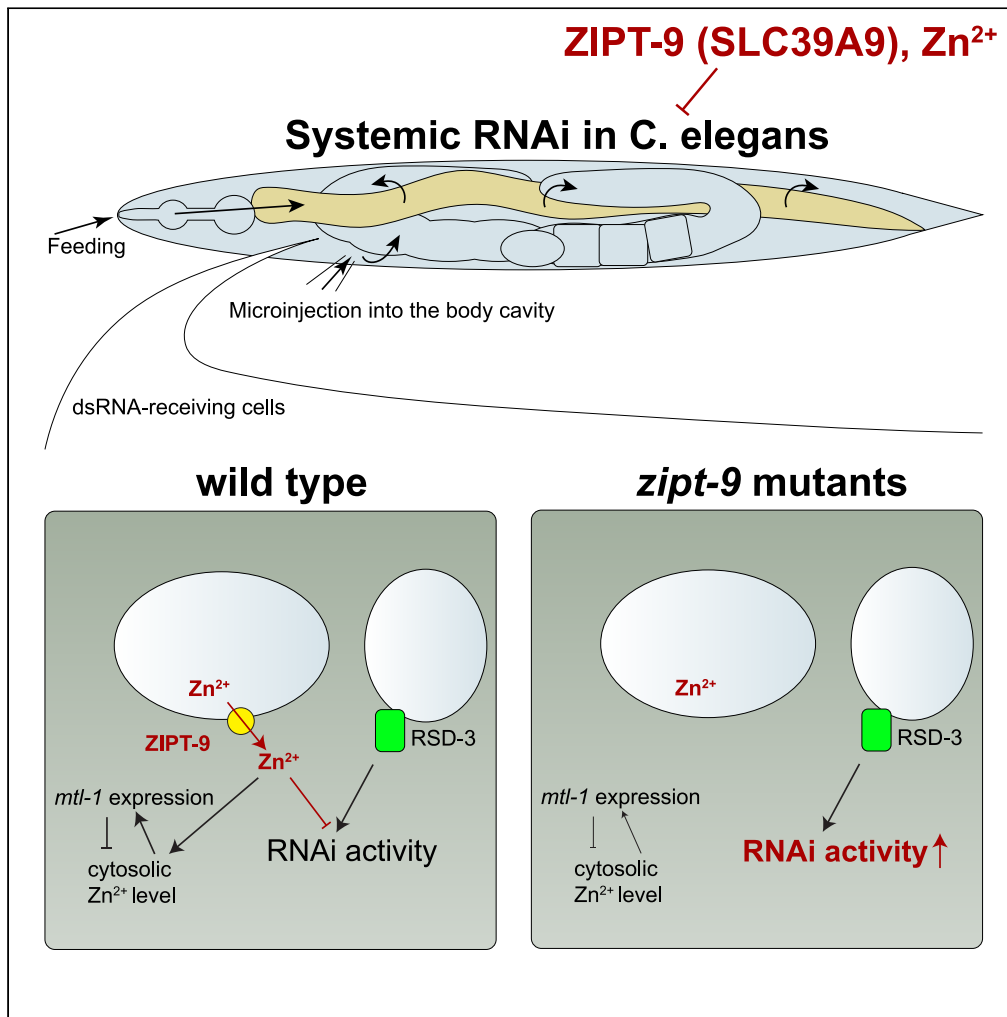


Article

An endomembrane zinc transporter negatively regulates systemic RNAi in *Caenorhabditis elegans*

Katsufumi Dejima,
Rieko Imae, Yuji
Suehiro, Keita
Yoshida, Shohei
Mitani

mitani.shohei@twmu.ac.jp

Highlights

zipt-9 was identified as a
suppressor of RNAi
defects of *rsd-3* mutants

ZIPT-9 predominantly
resides in late endosomes
and affects vesicle size

ZIPT-9 mutation restores
RNAi efficiency in multiple
RNAi-defective mutants

Zn²⁺ homeostasis via
ZIPT-9, not overall
cytosolic Zn²⁺, is the key
for systemic RNAi

Article

An endomembrane zinc transporter negatively regulates systemic RNAi in *Caenorhabditis elegans*Katsufumi Dejima,¹ Rieko Imae,¹ Yuji Suehiro,¹ Keita Yoshida,¹ and Shohei Mitani^{1,2,*}

SUMMARY

Double-stranded RNA (dsRNA) regulates gene expression in a sequence-dependent manner. In *Caenorhabditis elegans*, dsRNA spreads through the body and leads to systemic RNA silencing. Although several genes involved in systemic RNAi have been genetically identified, molecules that mediate systemic RNAi remain largely unknown. Here, we identified ZIPT-9, a *C. elegans* homolog of ZIP9/SLC39A9, as a broad-spectrum negative regulator of systemic RNAi. We showed that RSD-3, SID-3, and SID-5 genetically act in parallel for efficient RNAi, and that *zipt-9* mutants suppress the RNAi defects of all the mutants. Analysis of a complete set of deletion mutants for SLC30 and SLC39 family genes revealed that only *zipt-9* mutants showed altered RNAi activity. Based on these results and our analysis using transgenic Zn²⁺ reporters, we propose that ZIPT-9-dependent Zn²⁺ homeostasis, rather than overall cytosolic Zn²⁺, modulates systemic RNAi activity. Our findings reveal a previously unknown function of zinc transporters in negative RNAi regulation.

INTRODUCTION

Zinc is a trace metal element that binds to numerous proteins and serves as a cofactor in enzyme catalysis and protein stabilization.¹ In metazoans, two zinc transporter families, the SLC30/ZnT family and SLC39/ZIP family, play crucial roles in coordinating Zn²⁺ homeostasis by transporting Zn²⁺ across the biological membrane: SLC30 transports cytosolic Zn²⁺ to the extracellular space and into organelles, while SLC39 imports the ion to the cytoplasm.^{2,3} Mutations and abnormal expression of these zinc transporters are associated with immunity, cancer progression, and development. These zinc transporters seem to have specific physiological functions,⁴ highlighting the importance of understanding the specific roles of each transporter *in vivo*.

In *Caenorhabditis elegans*, exogenously administered double-stranded RNA (dsRNA) spreads over the whole body and leads to RNA silencing in a cell non-autonomous manner,⁵ the phenomenon of which is termed systemic RNAi. Previous studies have found that certain genes play a role in systemic RNAi.⁶ To silence genes, the cell needs to transport extracellular dsRNA into the cytosol where the RNA silencing machinery is located. The dsRNA-selective importer systemic RNAi defective-1 (SID-1) mediates passive cellular uptake of dsRNA.^{7,8} The mammalian SID-1 ortholog has also been shown to enable the transport of internalized dsRNA derived from the virus from endosomal compartments to the cytoplasm.⁹ Genetic studies using *C. elegans* and *Drosophila* S2 cells suggested that uptake of dsRNA occurs through clathrin-mediated endocytosis.¹⁰ However, there was some discrepancy in another study over whether clathrin-mediated endocytosis is required for positive regulation in RNAi,¹¹ implying that the relationship between clathrin-mediated endocytosis and systemic RNAi activity is complex. Given that loss of several endomembrane proteins, including SID-3 (ACK family tyrosine kinase homolog),¹² RSD-3 (epsinR homolog),^{13,14} SID-5 (nematode-specific late endosomal protein),¹⁵ and SEC-22 (late endosomal SNARE),¹⁶ was shown to lead to abnormalities in systemic RNAi in *C. elegans*, endomembrane trafficking must play some crucial roles in the spread of dsRNA. IP₃ signaling was also shown to modulate systemic RNAi sensitivity.¹⁷ SEC-22 negatively regulates RNAi in a SID-5-dependent manner.¹⁶ However, the connection of these positive RNAi factors, which are localized to endomembrane vesicles (RSD-3, SID-3, and SID-5), is unknown. In *C. elegans*, dsRNA ingested from food sources triggers systemic RNAi, the phenomenon of which is termed feeding RNAi.¹⁸ In feeding RNAi, the nematode-specific apical intestinal membrane protein SID-2 is required for the import of ingested dsRNA.^{19,20} SID-2 requires the basolateral recycling pathway involving SID-3 and its interactor EHBP-1.²¹ Of note, in *C. elegans*, the endogenous RNAi (endo-RNAi) pathway that plays a role in the regulation of gene expression antagonizes exogenous RNAi (exo-RNAi) in cells because it

¹Department of Physiology, Tokyo Women's Medical University School of Medicine, 8-1, Kawada-cho, Shinjuku-ku, Tokyo 162-8666, Japan

²Lead contact

*Correspondence:

mitani.shohei@twmu.ac.jp

<https://doi.org/10.1016/j.isci.2023.106930>



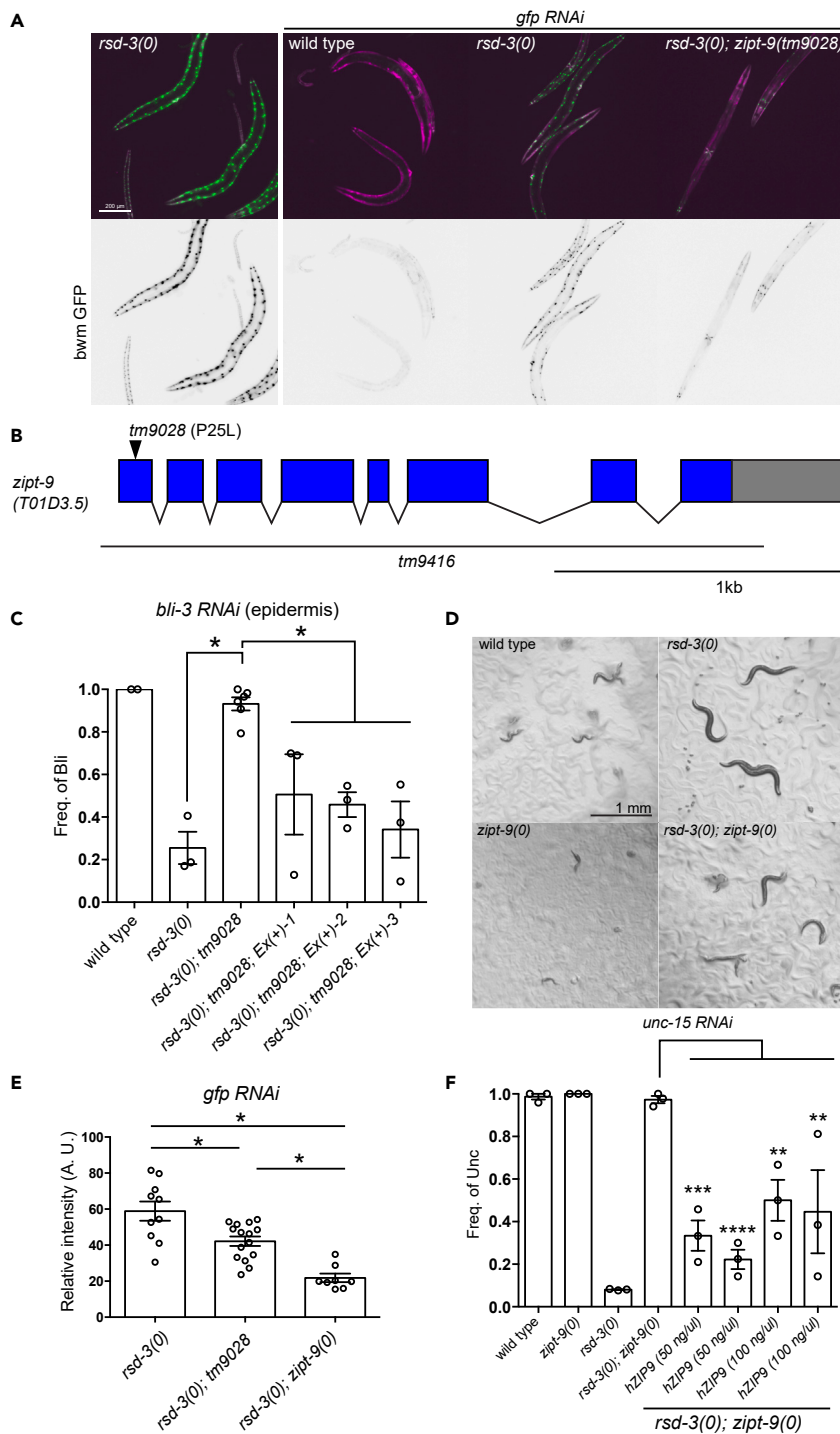


Figure 1. ZIPT-9 negatively regulates systemic RNAi

(A) Suppressor mutants for *rsd-3* show enhanced sensitivity to GFP feeding RNAi. Representative wild-type, *rsd-3(0)* and *tm9028; rsd-3(0)* animals subjected to L4440 vector control feeding RNAi (left) or GFP RNAi (right three panels). Scale bar: 200 μ m.

(B) Gene structure of *zipt-9* (T01B3.5) showing mutations in isolated alleles. Sequence deleted in *zipt-9(tm9416)* is indicated by a solid line.

(C) Suppressor mutants for *rsd-3* show enhanced sensitivity to *bli-3* feeding RNAi, and *zipt-9* (T01B3.5) genomic fragment rescues the suppressor phenotype. For the rescue experiment, three independent transgenic strains (*Ex(+)-1*: *tmEx4305*,

Figure 1. Continued

Ex(+)-2: *tmEx4306*, Ex(+)-3: *tmEx4307*), were tested. Bars represent the mean frequency (\pm SEM) of animals showing the blister (Bli) and/or larval arrest (Lva) phenotypes from several independent experiments. * $p < 0.05$.

(D) Embryos were placed on plates seeded with bacteria without dsRNA (mock) or bacteria expressing *bli-3* dsRNA, and photographed 72 h later. Wild-type and *zipt-9(0)* animals fed on food containing *bli-3* dsRNA showed a severe Bli phenotype and resulted in a larval arrest at L2~L3 stage, whereas almost all *rsd-3(tm9006)* worms reached adulthood. The animals of double mutant animals for *rsd-3* and *zipt-9* showed a milder Bli phenotype and resulted in the larval arrest at L3~L4 stage. Scale bar: 1 mm.

(E) *zipt-9(0)* exhibits stronger suppressor effect on *gfp* feeding RNAi than *zipt-9(tm9028)*. Bars represent mean intensity of GFP signal in arbitrary units (a.u.). * $p < 0.05$.

(F) Expression of hZIP9 under the control of *zipt-9* promoter rescues the suppressor phenotype of *zipt-9(0)*. The results of *unc-15* feeding RNAi are shown. The partial rescue was observed on *bli-3* RNAi (Figure S2E). Bars represent the mean frequency (\pm SEM) of animals showing the uncoordinated (Unc) phenotype from several independent experiments. ** $p < 0.01$, *** $p < 0.005$, **** $p < 0.001$.

competes with several RNA silencing machineries in the exo-RNAi pathway.^{22,23} ARF-like small GTPase ARL-8, which functions in endosome-to-lysosome trafficking, was shown to be required for spermatogenesis-specific endogenous siRNA production and negatively affect both somatic and germline exo-RNAi activity.^{11,24} Thus, systemic RNAi consists of several regulatory mechanisms, both through positive and negative regulation. Because many molecules described above are conserved in wide taxonomic ranges, the molecular mechanisms underlying the systemic spreading of dsRNA in *C. elegans* appear to be conserved, at least partly, among plants, invertebrates, and vertebrates.²⁵ Cellular pathways and molecules that mediate systemic RNAi through negative regulation remain largely unknown.

Here, using an unbiased genetic screen, we identified ZIPT-9, a *C. elegans* homolog of Zrt Irt-like protein 9 (ZIP9/SLC39A9), as a negative regulator that extensively affects systemic RNAi. Our results suggest that ZIPT-9 is involved in endomembrane trafficking regulation. Analysis of a complete set of deletion mutants for SLC30 and SLC39 family genes revealed that *zipt-9* mutants showed altered RNAi activity under normal culture conditions, and these were the only mutations among zinc transporters that showed this change. Our findings provide the first example of Zn²⁺ and its transporter acting in the negative regulation of RNAi.

RESULTS***zipt-9* mutants suppress the RNAi-defective phenotype of *rsd-3* mutants**

We previously showed that RSD-3/EpsinR is required for the import of exogenously administered dsRNA, and loss of this protein causes a partial defect in systemic RNAi.^{13,14} However, the known molecules, including RSD-3, do not fully explain the mechanism of silencing RNA uptake for efficient systemic RNAi. To identify novel components modulating systemic RNAi, we performed a forward genetic screen in which mutants suppressed the RNAi defects of *rsd-3* mutants. The *rsd-3* null mutant strain that was used to identify the suppressors expressed GFP and red fluorescent protein (mCherry) in body wall muscle (bwm) cells. After performing EMS mutagenesis, we examined their response to *gfp* feeding RNAi,¹⁸ which induces systemic silencing of GFP through spread of the fed dsRNA targeting *gfp* from the intestine, and sought animals in which bwm GFP but not mCherry signal was reduced (Figure 1A). We found a recessive suppressor mutation in a zinc importer SLC39 family gene, *zipt-9*, a *C. elegans* homolog of ZIP9. The suppressor allele *tm9028* has a homozygous G to A transition at 23,637 in the cosmid T01D3, resulting in a proline25 to leucine amino acid substitution in the *zipt-9/T01D3.5* gene (Figures 1B and S2A). The restoration of sensitivity to feeding RNAi in the suppressor strain was further confirmed by RNAi targeting endogenous genes; the isolated strain was sensitive to *bli-3*, *unc-15*, and *pos-1* RNAi, which led to epidermal (blister, Bli), muscular (uncoordinated, Unc), and germline (embryonic lethal, Emb) phenotypes in wild-type animals, respectively, (Figures 1C, S2B, and S2C). The effect of suppression on the feeding RNAi defects was rescued by the introduction of wild-type *zipt-9* genomic PCR fragment and expression of the *zipt-9* cDNA-tagRFP fusion protein under the control of its own or intestinal promoter (Figures 1C and S2D). To further confirm that *zipt-9* is the causal suppressor gene, we isolated a deletion allele for this gene using the CRISPR-Cas9 method^{26,27} (Figure 1B). The isolated deletion allele *tm9416* completely lacked the coding sequence and suppressed the RNAi-defective phenotype of *rsd-3* mutant animals (Figure 1D). We refer to *tm9416* as *zipt-9(0)* in the following sections. The suppression effect of *zipt-9(0)* was stronger than that of *tm9028*, suggesting that the P25L mutation was a partial loss of function (Figure 1E). In addition, we found that the human ZIPT-9 ortholog hZIP9 partially rescued the suppressor phenotype (Figures 1F and S2E), suggesting functional conservation between *C. elegans* ZIPT-9 and mammalian ZIP9. From these experiments, we conclude that *zipt-9* is the causal gene of the suppressor phenotype.

ZIPT-9 functions in systemic RNAi through its zinc transporter activity

To determine whether Zn^{2+} homeostasis is affected in *zipt-9(0)* mutants, we first tested the promoter activity of a metallothionein gene, *mtl-1*, using *Pmtl-1::gfp*, which is induced by excess dietary Zn^{2+} .²⁸ We observed a decrease in *Pmtl-1::gfp* expression in *zipt-9(0)* mutants with no supplemental Zn^{2+} (Figures 2A and 2B). The induction of *Pmtl-1::gfp* in *zipt-9(0)* mutants was much milder than that in wild-type animals in the presence of either low or high concentrations of supplemental Zn^{2+} (Figures 2A and 2B). These data indicate that the transcriptional response to excess Zn^{2+} , which is expected to reduce intracellular free Zn^{2+} levels, is weakened in *zipt-9(0)*. The reduced transcriptional response to excess Zn^{2+} could be due to Zn^{2+} import defects. To estimate the cytosolic free Zn^{2+} level more directly, we employed a Förster resonance energy transfer (FRET)-based Zn^{2+} sensor ZapCY2.²⁹ The FRET signal in wild-type animals was transiently increased 1 h after exposure to high concentrations of Zn^{2+} (Figures 2C and 2D). This transient increase in the FRET signal was weak in *zipt-9(0)* mutants, suggesting that ZIPT-9 mediates acute Zn^{2+} import into the cytosol in the presence of high environmental Zn^{2+} (Figures 2C and 2D). We found that the FRET signal was not affected in the mutant under normal culture conditions (0-h time point) and after the time point when wild-type animals showed a transient increase in the FRET signal (2-h time point). In addition, longer exposure to high supplemental Zn^{2+} resulted in a slight but significantly different increase in the FRET signal in *zipt-9(0)* mutants (6-h time point). Because we observed repression of *Pmtl-1::gfp* in the mutant as described above (Figures 2A and 2B), the lack of a significant change in the FRET signal at the 0-h time point could be due to compensation by transcriptional repression of some Zn^{2+} regulators including MTL-1, upon reduced Zn^{2+} import activity.

The histidine residues in transmembrane domain 4 (TMD4) and TMD5 of the SLC39A family are predicted to be intramembranous zinc-binding sites.³ To test whether ZIPT-9 functions in systemic RNAi via its Zn^{2+} transport activity, we created mutant forms of ZIPT-9 and examined whether the expression of the mutant ZIPT-9 proteins could rescue the suppressor phenotype. The replacement of either or both conserved histidine 217 in TMD4 or histidine 247 in TMD5 with alanine showed no rescue (Figure 2E). These data suggested that ZIPT-9 acts in systemic RNAi through its zinc transporter activity. Given that *zipt-9* mutants suppressed the RNAi-defective (Rde) phenotype of *rsd-3(0)*, one possibility was that RSD-3 might negatively regulate ZIPT-9 function, and highly activated ZIPT-9 in *rsd-3(0)* could lead to systemic RNAi defects. However, we excluded this possibility and favored the idea that ZIPT-9 could act in parallel with or antagonistic to RSD-3 because *Pmtl-1::gfp* expression in the *rsd-3(0)* mutant was normal (Figures 2A and 2B).

ZIPT-9 negatively regulates exo-RNAi by a mechanism other than that associated with reduced activity of the endo-RNAi pathway

As RSD-3 does not appear to inhibit the function of ZIPT-9, we next investigated whether ZIPT-9 plays a negative role in systemic RNAi in the presence of RSD-3. We analyzed the sensitivity of the *zipt-9* single mutant toward feeding RNAi targeting *unc-73* (a neuronal gene, and its loss induces the Unc phenotype), *hmr-1* (an embryonic epidermal gene, and its loss induces the maternal body morphology defect phenotype), *dpy-13* (an epidermal gene, and its loss induces a dumpy phenotype), and *lin-1* (a vulval precursor gene, and its loss induces abnormal vulval development), which confer low-penetrant RNAi effects in wild-type animals.³⁰ The *zipt-9(0)* single mutants were more sensitive to *hmr-1*, *dpy-13*, and *lin-1* RNAi than the wild type, suggesting that ZIPT-9 itself negatively functions in systemic RNAi (Figures 3A–3D). Previous studies have shown that inhibition of the genes involved in the endo-RNAi pathway that are antagonistic to the exo-RNAi pathway results in an enhanced RNAi (Eri) phenotype.²² To test the relationship between ZIPT-9 and the endo-RNAi pathway, we examined the genetic interaction between *zipt-9* and *rff-3*, which encodes an RNA-dependent RNA polymerase required for amplification of endogenous siRNA.³⁰ The double mutant for *zipt-9(0)* and *rff-3(tm6937)* showed a stronger Eri phenotype than each single mutant (Figure 3E). We also found a phenotypic difference between mutants of *zipt-9* and *eri-1*, a gene encoding an exonuclease required for degradation of endogenous siRNA. While mutants of *eri-1* show more sensitivity to feeding RNAi targeting *unc-73* than wild type, as reported previously,²² *zipt-9(0)* did not (Figure 3A). In addition, *zipt-9(0)* was fertile at high temperature, whereas *eri-1* mutants displayed sterility (Figure 3F). Consistent with these results, RT-qPCR analysis revealed that expression of the endo-RNAi target genes was not affected in *zipt-9(0)* (Figures 3G and 3H). Thus, although the *zipt-9* single mutant partly phenocopied the mutants for the endo-RNAi pathway in terms of enhanced RNAi sensitivity, ZIPT-9 negatively regulates exo-RNAi mainly by a mechanism other than that associated with reduced activity of the endo-RNAi pathway.

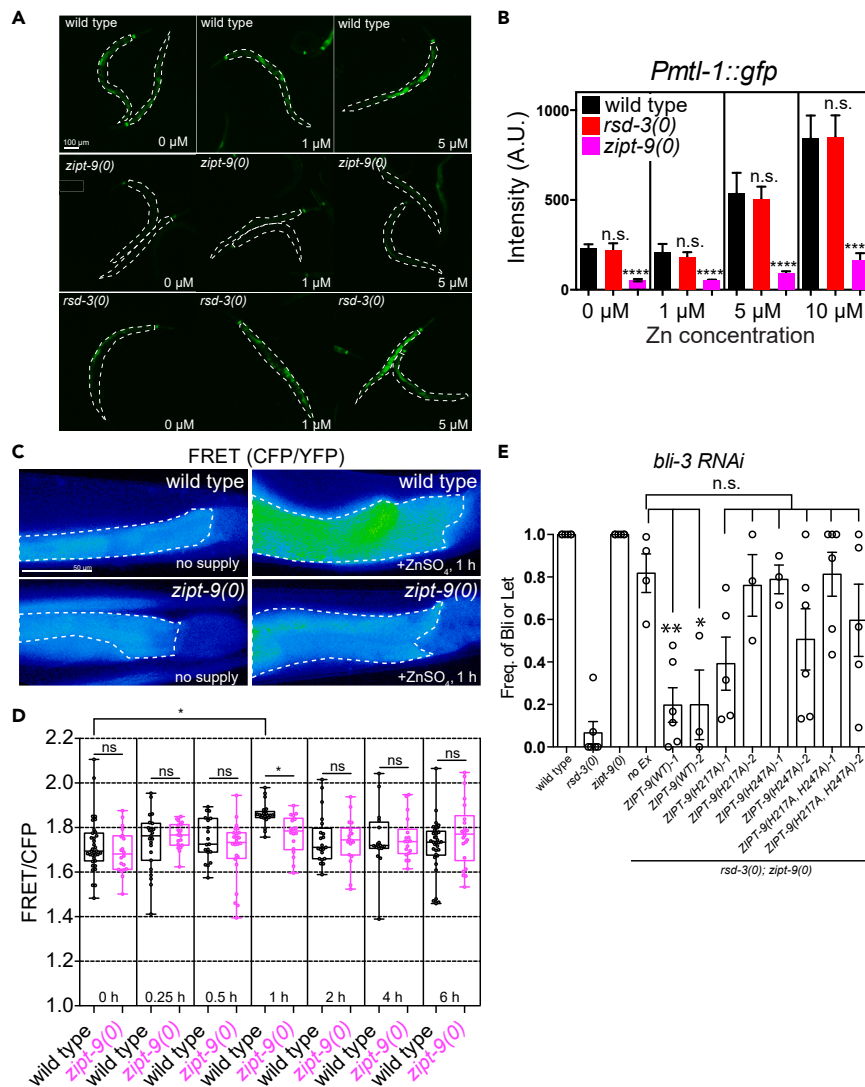


Figure 2. ZIPT-9 functions in systemic RNAi through its zinc transporter activity

(A and B) Fluorescence microscope images of transgenic hermaphrodites expressing GFP under the control of the *mtl-1* promoter (*tmEx4662[Pmtl-1::gfp]*). The animals of the indicated genotype were cultured on noble agar plates with 0, 1, or 5 μ M supplemental zinc. $n = 15$ – 29 . Scale bar: 100 μ m. **** $p < 0.001$, n.s., not significant.

(C) Representative pseudo-colored FRET ratio images of the posterior intestine in transgenic hermaphrodites expressing Zn^{2+} sensor under the control of the *vha-6* promoter (*tmEx4758[Pvha-6::NES-ZapCY2]*). The images were created by dividing FRET pixel intensity values by ECFP pixel intensity values. Scale bar: 50 μ m.

(D) Time course analysis of NES-ZapCY2 FRET levels in wild-type and *zip1-9(0)* animals. The day-one adult worms of the indicated genotype were cultured on NGM agar plates with 2.8 mM supplemental Zn^{2+} and imaged at each time point. Values are obtained by FRET pixel intensity values by ECFP pixel intensity values. Error bars represent \pm SEM. * $p < 0.05$. n.s., not significant.

(E) Expression of wild-type (WT) but not mutant (H217A, H274A, or H217A H274A) form of ZIPT-9 under the control of *vha-6* promoter rescues the suppressor phenotype of *zip1-9(0)*. The results of *bli-3* feeding RNAi are shown. Bars represent the mean frequency (\pm SEM) of animals showing Bli phenotype from several independent experiments. * $p < 0.05$. ** $p < 0.01$. n.s., not significant.

ZIPT-9 is predominantly localized to late endosomes and affects the size of vesicles associated with RAB-5, FYVE-domain, RAB-7, and LMP-1

We found that ZIPT-9 was widely expressed in the pharynx, intestine, and epidermis throughout development (Figure 4A). The localization of ZIPT-9 was correlated with RAB-7-positive late endosomes/MVBs and

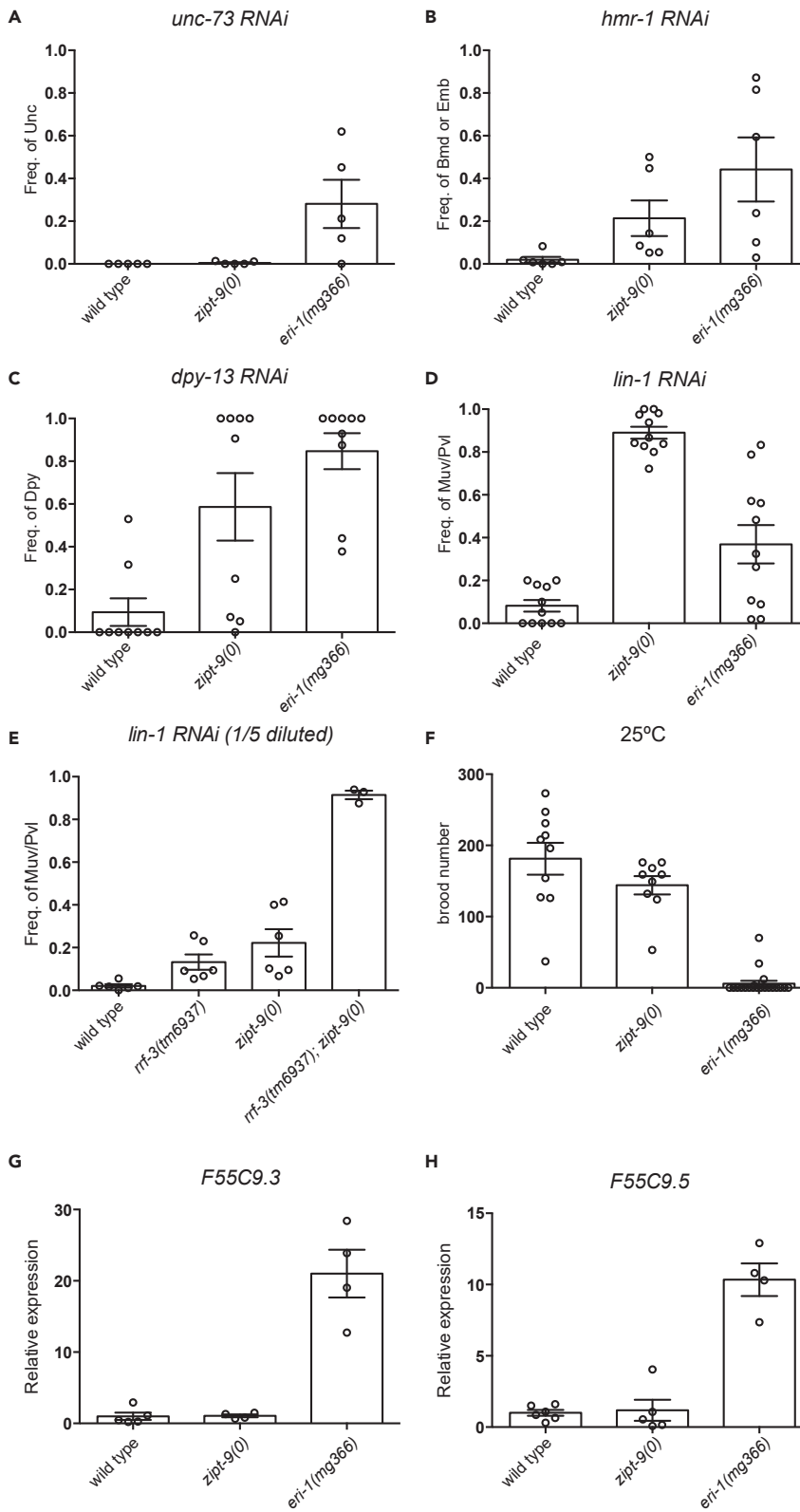


Figure 3. ZIPT-9 negatively regulates exo-RNAi by a mechanism other than that associated with reduced activity of the endo-RNAi pathway

(A) Mutants for *eri-1* but not *zipt-9* are sensitive to *unc-73* RNAi induced by feeding. Bars represent the mean frequency (\pm SEM) of animals showing Unc phenotype from several independent experiments.

(B) Both *eri-1* and *zipt-9* mutants are sensitive to *hmr-1* RNAi induced by feeding. Bars represent the mean frequency (\pm SEM) of animals showing body morphology defect (Bmd) phenotype from several independent experiments.

(C) Both *eri-1* and *zipt-9* mutants are sensitive to *dpy-13* RNAi induced by feeding. Bars represent the mean frequency (\pm SEM) of animals showing Dpy phenotype from several independent experiments.

(D) Both *eri-1* and *zipt-9* mutants are sensitive to *lin-1* RNAi induced by feeding. Bars represent the mean frequency (\pm SEM) of animals showing multi-vulva (Mvl) or pultruding vulva (Pvl) phenotype from several independent experiments.

(E) The double mutants for *zipt-9(0)* and *rrf-3(tm6937)* are more sensitive to *lin-1* feeding RNAi in which HT115 expressing *lin-1* dsRNA is diluted to 1:5 in LB than every single mutant. Bars represent the mean frequency (\pm SEM) of animals showing Mvl or Pvl phenotype from several independent experiments.

(F) *zipt-9(0)* is fertile at 25°C, while *eri-1(mg366)* displays temperature-dependent sterility.

(G and H) RT-qPCR showing relative expression levels of F55C9.3 (G) and F55C9.5 (H) mRNA normalized to *ama-1* expression. RNA was extracted from young-adult animals grown at 20°C. Bars represent the mean from independent samples (\pm SEM). Fold changes were normalized by the value of wild-type animals.

weakly correlated with RAB-5-positive early and RAB-11-positive recycling endosomes (Figures 4B and 4C). While ZIPT-9 is the homolog of ZIP9 that is localized to the Golgi apparatus³¹ and lysosome, ZIPT-9 weakly colocalized with the Golgi marker AMAN-2 and lysosomal marker LMP-1³² (Figures 4B and 4C). These results indicated that ZIPT-9 is predominantly localized to late endosomes in *C. elegans*. Given that ZIPT-9 does not function through regulation of the endo-RNAi pathway and that endosome-associated proteins, including RSD-3, SID-3, SEC-22, and SID-5, function in systemic RNAi, we hypothesized that ZIPT-9 participates in the regulation of endosomal trafficking. To test this hypothesis, we examined the morphology of endosomes and lysosomes in coelomocytes that have easy-to-observe early and late endosomes and lysosomes.³³ We found that the *zipt-9(0)* mutants had larger FYVE-positive early endosomes and RAB-7-positive late endosomes (Figures 4D–4G). In contrast, *zipt-9(0)* mutants showed smaller LMP-1-positive lysosomes (Figures 4H and 4I). In addition, unusual RAB-5 signals were found on large vesicles in the *zipt-9(0)* mutant day 1 adult intestine (Figure 4J). These data suggested that loss of ZIPT-9 leads to less trafficking to vesicles associated with LMP-1 from FYVE- or RAB-5-positive early endosomes and RAB-7-positive late endosomes where ZIPT-9 is predominantly localized.

ZIPT-9 negatively regulates systemic RNAi through multiple mechanisms

To determine how ZIPT-9 functions in the systemic RNAi pathway, we performed genetic epistasis analysis between *zipt-9* and known mutants defective in systemic RNAi. We created double mutants for *zipt-9* and six genes involved in systemic RNAi: four systemic RNAi-defective (*sid*) genes, *sid-1*, *sid-2*, *sid-3*, and *sid-5*, inositol-phosphate phosphatase, *ipp-5*, an inhibitory factor for IP₃ signaling that negatively regulates systemic RNAi,¹⁷ and *sec-22*, which was shown to act as a negative regulator in systemic RNAi. We found that *sid-1* and *sid-2* were epistatic to *zipt-9* for sensitivity to *bli-3*, *unc-15*, and *pos-1* feeding RNAi, suggesting that SID-1 and SID-2 are essential for RNAi, the efficiency of which can be modulated through ZIPT-9 (Figures 5A–5C). In contrast, *zipt-9(0)* suppressed the RNAi-defective phenotype caused by loss of function in *sid-3* or *sid-5* (Figures 5A–5C). The Eri phenotype of *sec-22(ok2053)* was much milder than that of *zipt-9(0)*, and that of the double mutant for these genes was comparable to that of the *zipt-9(0)* single mutant, suggesting that the ZIPT-9-dependent mechanisms may include the SEC-22-dependent mechanism (Figure 5D). Loss of function of *zipt-9* showed a synthetic growth defect with that in *ipp-5*, so we could not determine the epistasis of these genes (Figure 5E). Given our findings that *zipt-9(0)* suppressed the RNAi defects caused by each *sid-3*, *sid-5*, or *rsd-3* mutation, we then examined the genetic interaction of these RNAi-defective genes. We found enhancement of the RNAi defects in all the combinations (Figure 5F). Although we could not exclude the possibility that SID-3, SID-5, and RSD-3 function on a single pathway and that the synergistic RNAi defect was caused by a greater effect in inhibiting this pathway when two of them were disrupted, we favored the idea that these act in systemic RNAi in parallel pathways or through different mechanisms. Because of this synergistic effect among RSD-3, SID-3, and SID-5 and the lower selectivity of *zipt-9(0)* to these mutants for suppression, our genetic interaction experiments indicated that ZIPT-9 negatively regulates systemic RNAi through multiple mechanisms. Alternatively, ZIPT-9 may negatively affect the fundamental cellular physiological status required for systemic RNAi.

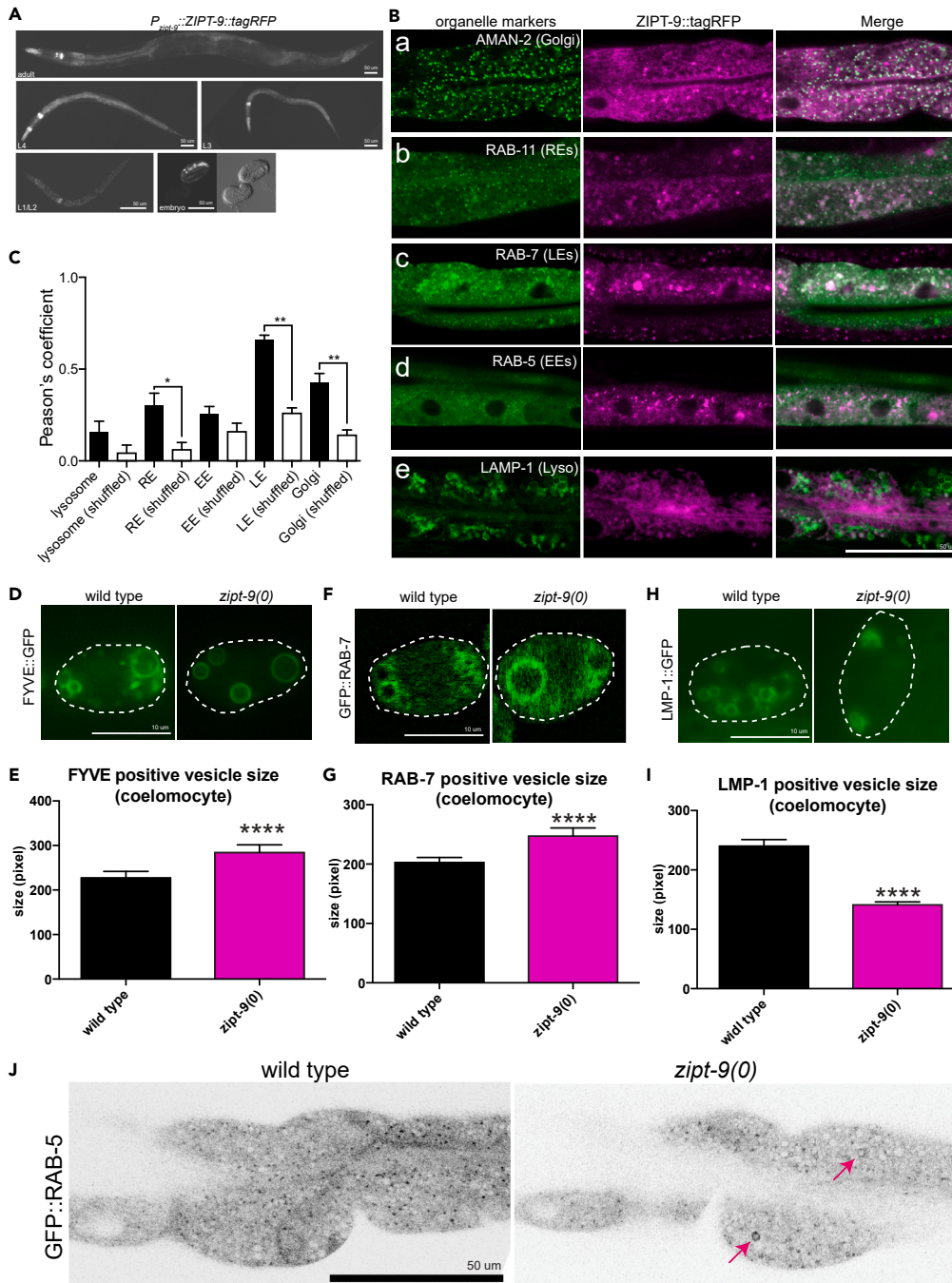


Figure 4. ZIPT-9 is predominantly localized to late endosomes and affects the size of vesicles associated with RAB-5, FYVE-domain, RAB-7, and LMP-1

(A) Fluorescent images of adult, L4, L3, L2, and embryonic stage animals expressing ZIPT-9::tagRFP under the control of *zipt-9* own promoter. Scale bars: 50 μ m.

(B) Subcellular localization of tagRFP-tagged ZIPT-9 in the intestinal cells. Shown are confocal images of the anterior intestine of L4 stage animals expressing ZIPT-9::tagRFP and AMAN-2::GFP (a), RAB-11::GFP (b), GFP::RAB-7 (c), GFP::RAB-5 (d), and LMP-1::GFP (e). Scale bar: 50 μ m.

(C) Colocalization coefficients (Pearson's coefficients) between ZIPT-9::tagRFP and GFP-tagged organelle markers. The images from red and green channels were randomly shuffled and correlation of pixels between the two channels was obtained as controls (shuffled control). Statistical differences (p values) of coefficients between two channels from original

Figure 4. Continued

and shuffled images were calculated using a two tailed unpaired Student's t test. * $p < 0.05$. ** $p < 0.01$. Error bars represent \pm SEM.

(D) Fluorescence images showing FYVE-associated vesicles in coelomocytes from L4 animals. Scale bar: 10 μ m.

(E) Size of FYVE-associated vesicles in wild type and *zipt-9(0)*. Images of 20 coelomocytes were analyzed for each strain. p values were calculated using a two-tailed unpaired Student's t-test. **** $p < 0.001$. Error bars represent \pm SEM.

(F) Confocal fluorescence images showing RAB-7-associated vesicles in coelomocytes from L4 animals. Scale bar: 10 μ m.

(G) Size of RAB-7-associated vesicles in wild type and *zipt-9(0)*. Images of 20 coelomocytes were analyzed for each strain. p values were calculated using a two-tailed unpaired Student's t-test.

(H) Fluorescence images showing LMP-1-associated vesicles in coelomocytes from L4 animals. Scale bar: 10 μ m.

(I) LMP-1-associated vesicle size in wild type and *zipt-9(0)*. For each strain, images of 20 coelomocytes were analyzed. p values were calculated using a two tailed unpaired Student's t test.

(J) Confocal fluorescence images showing RAB-5-associated vesicles in the anterior intestine of young adult animals. Arrowheads indicate large vesicles found in *zipt-9(0)* but not in wild type. Scale bar: 50 μ m.

ZIPT-9 functions at least in dsRNA import or more downstream events in dsRNA-recipient germ cells

Previous studies suggested that SID-3 and RSD-3 function mainly, if not exclusively, in the import of silencing RNA,^{12,14} while SID-5 functions in the export.¹⁵ Our genetic interaction experiments suggested that ZIPT-9 could act in both processes. Further experiments supported the view that ZIPT-9 acts at least in dsRNA import or more downstream in the import of silencing RNA in dsRNA-receiving cells. In feeding RNAi, the long dsRNA is ingested by intestinal cells and then exported to the pseudocoelom. Unprocessed long dsRNA, rather than short dsRNA processed by machinery including RDE-4 and DCR-1, is exported and imported into somatic and germ cells.³⁴ To address which process of dsRNA traffic is enhanced in *zipt-9(0)* animals, we examined whether in the absence of ZIPT-9, the long dsRNA injected into the pseudocoelom can silence its target gene expression more efficiently. We injected *pos-1* dsRNA into the pseudocoelom and scored the Emb phenotype of progeny produced from the injected animals. Consistent with our previous report,¹⁴ *rsd-3(0)* showed partial resistance to *pos-1* dsRNA injection, suggesting that the efficiency of dsRNA import was reduced in *rsd-3(0)* mutants. We found that *zipt-9(0)* significantly suppressed this defect (Figures 6A and 6B), suggesting that ZIPT-9 functions at least in dsRNA import or more downstream events in dsRNA-recipient germ cells.

Zn²⁺ imported through ZIPT-9 is distinctive from that of the other zinc transporters

Loss of ZIPT-9 activity could cause an increase in free Zn²⁺ levels in the extracellular space or intracellular luminal compartments accompanied by a decrease in cytosolic free Zn²⁺ levels. To distinguish which consequence was correlated with the enhancement of dsRNA import activity, which was caused by loss of ZIPT-9, we injected the Zn²⁺-specific and cell-penetrating chelator N,N,N',N'-tetrakis (2-pyridylmethyl) ethylenediamine (TPEN) together with *pos-1* dsRNA into the pseudocoelom. Injection of *pos-1* dsRNA with TPEN increased the penetrance of embryonic lethality in wild-type animals, indicating that the decrease in cytosolic Zn²⁺ level impacts dsRNA import (Figure 6C). We next asked if zinc transporters other than ZIPT-9 are associated with RNAi efficiency. *C. elegans* has 14 predicted genes of both the ZIP and ZnT families.³ Of these, 13 genes have already been knocked out by the national bioresource project and *C. elegans* knockout consortium. We created deletion mutants for the remaining 7 ZIP and 7 ZnT genes using CRISPR-Cas9 and tested the RNAi sensitivity of these single mutants and double mutants with *rsd-3(0)*. These knockout worms showed neither resistance nor increased sensitivity to *bli-3* or *pos-1* feeding RNAi (Table 1). The intestinal zinc exporters CDF-2 and TTM-1 were reported to be redundantly important for Zn²⁺ homeostasis.²⁸ To test the possibility of redundancy between zinc exporters that may have an opposite effect on RNAi to ZIPT-9, we created double mutants for *cdf-2* and *ttn-1* and tested if they show the Rde phenotype. However, these double mutants also exhibited normal responses to *bli-3* and *pos-1* feeding RNAi (Figures 6D and 6E). Taken together, these results demonstrated that whereas cytosolic Zn²⁺ has an inhibitory effect on dsRNA import, Zn²⁺ imported by ZIPT-9 is distinctive from that imported by the other zinc transporters in terms of site of action.

Finally, to more directly investigate the involvement of zinc in RNAi, we conducted an experiment where zinc was added to the RNAi plate to determine its effect on *bli-3* RNAi. We found that the addition of zinc had no significant impact on wild type and *zipt-9* mutants (Figure 7). However, in the *rsd-3* mutants, zinc caused a significant reduction in the efficiency of RNAi. The suppressive effect of the *zipt-9* mutation in *rsd-3* mutants was partially attenuated by the addition of zinc. We also examined the effects of other metals but did not observe

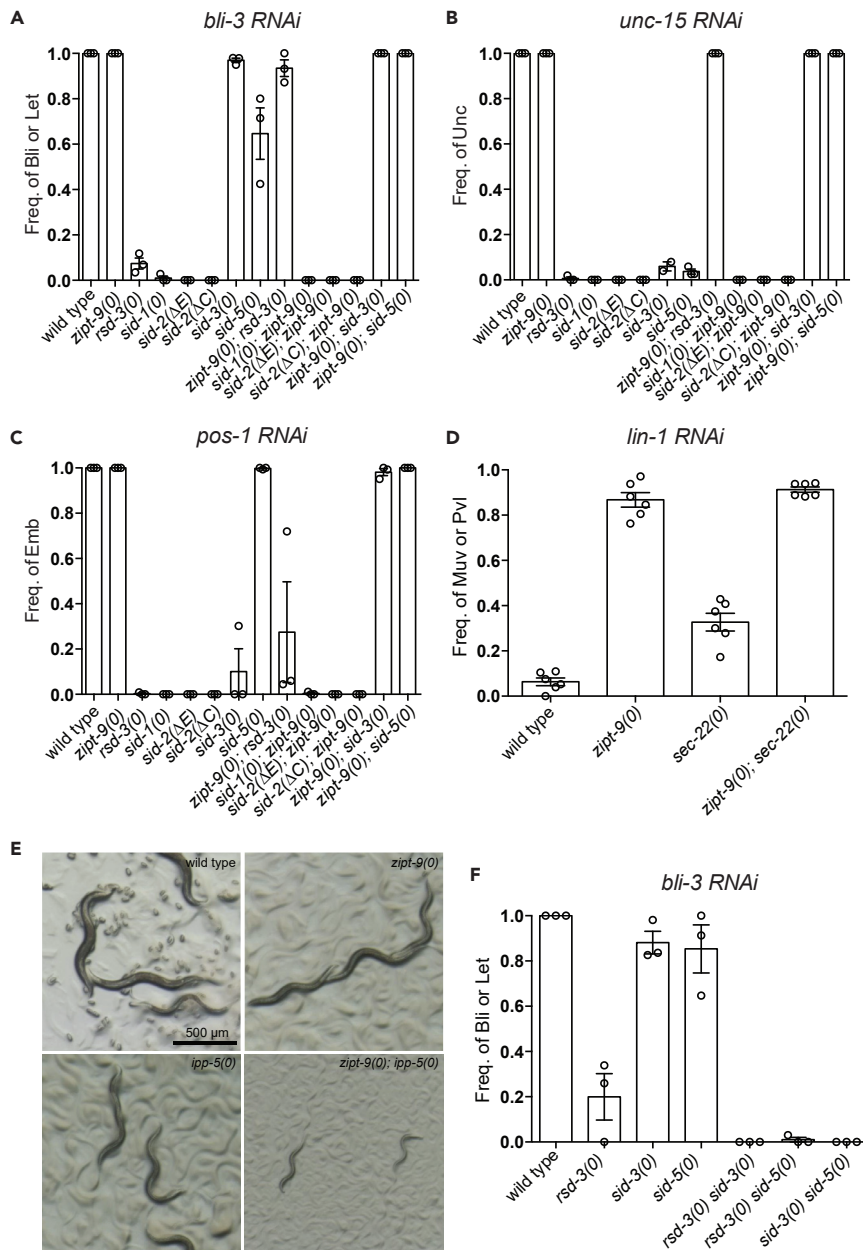


Figure 5. ZIPT-9 negatively regulates systemic RNAi through multiple mechanisms

(A) Quantification of the frequency of indicated mutant animals showing Bli phenotype under *bli-3* feeding RNAi. Bars represent the mean frequency (\pm SEM) of animals showing each phenotype from multiple independent experiments (A–D and F). The alleles used in Figure 5 are *rsd-3(0)*: *tm9006*, *sid-1(0)*: *tm2700*, *sid-2(ΔE)*: *tm9593*, *sid-2(ΔC)*: *tm9591*, *sid-3(0)*: *tm342*, *sid-5(0)*: *tm4328*, and *sec-22(0)*: *ok3053*.

(B) Quantification of the frequency of indicated mutant animals showing the Unc phenotype under *unc-15* feeding RNAi. Error bars represent \pm SEM.

(C) Quantification of the frequency of indicated mutant animals showing the Emb phenotype under *pos-1* feeding RNAi. Error bars represent \pm SEM.

(D) Quantification of the frequency of indicated mutant animals showing the Pvl or Muv phenotype under *lin-1* feeding RNAi. Error bars represent \pm SEM.

(E) Mutants for *zip-9* and *ipp-5* show weak slow growth phenotype. The double mutants of these genes show severe growth defects but are viable. Scale bars: 500 μ m.

(F) Quantification of the frequency of indicated mutant animals showing the Bli phenotype under *bli-3* feeding RNAi. Error bars represent \pm SEM.

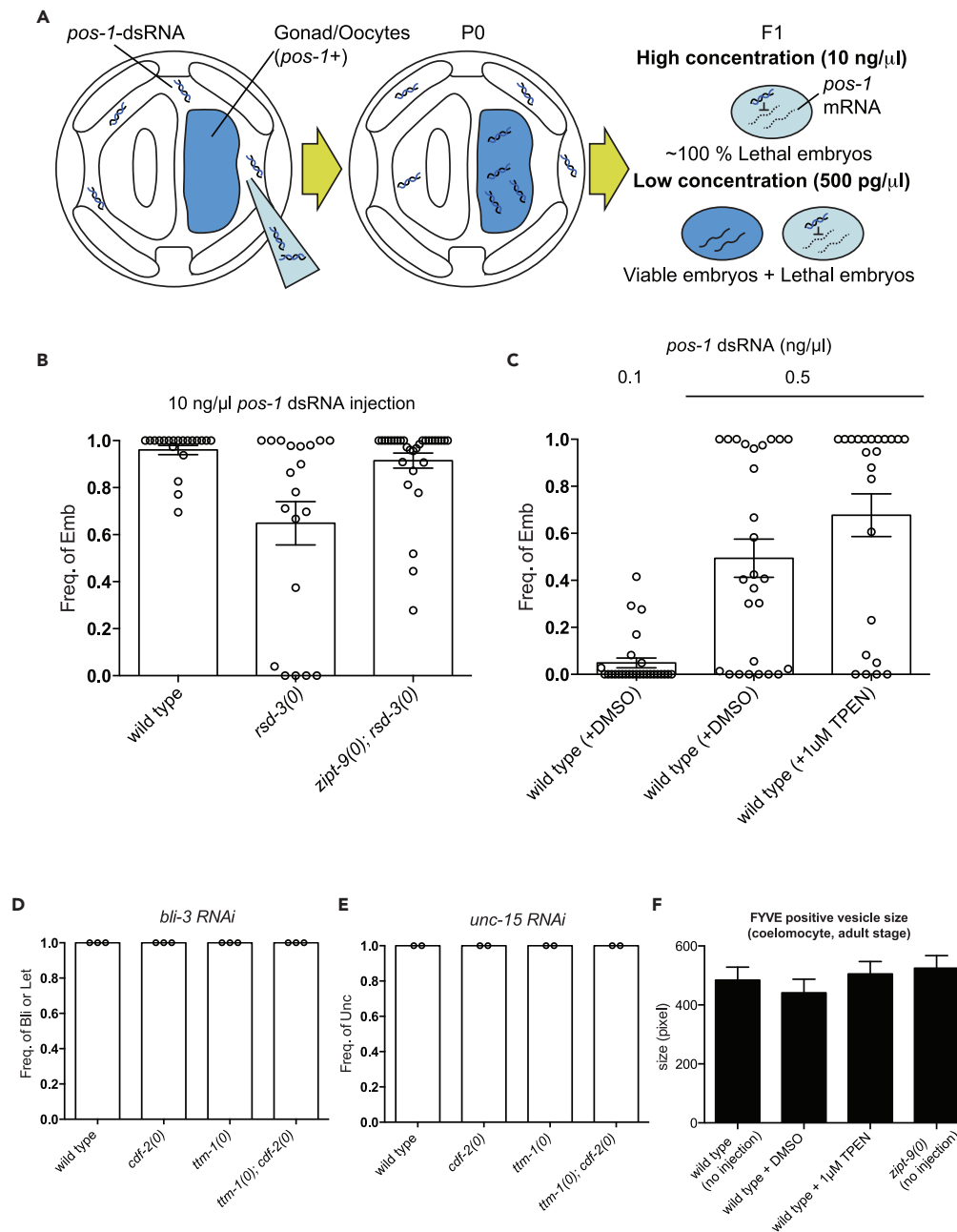


Figure 6. ZIPT-9 functions at least in dsRNA import or more downstream events in the dsRNA-recipient germ cells

(A) Schema of RNAi experiments by pseudocoelomic injection. Two different concentrations of dsRNA (high concentration: 10 ng/ μ L and low concentration: 500 pg/ μ L) targeting the *pos-1* gene, which is expressed in the germline, were injected into pseudocoelom of parent hermaphrodites, and the frequencies of F1 animal showing Emb phenotype were examined. Injection of low concentration *pos-1* dsRNA into the pseudocoelom induces about half penetrant Emb phenotype in the wild type (B). Injection of a high concentration of *pos-1* dsRNA into the pseudocoelom induces almost fully penetrant Emb phenotype in the wild type (C). Low concentration injection was used to examine if animals are more sensitive to RNAi than control animals (wild type with DMSO).

(B) Quantification of the frequency of indicated animals showing the Emb phenotype in F1 progeny derived from hermaphrodite pseudocoelomically injected with high concentration of *pos-1* dsRNA. Bars represent the mean frequency (\pm SEM) of animals showing each phenotype from several independent experiments.

(C) Quantification of the frequency of indicated animals showing the Emb phenotype in F1 progeny derived from hermaphrodite pseudocoelomically injected with low concentration of *pos-1* dsRNA in the presence or absence of TPEN. Bars represent the mean frequency (\pm SEM) of animals showing each phenotype from several independent experiments.

Figure 6. Continued

(D) Quantification of the frequency of indicated mutant animals showing the Bli phenotype under *bli-3* feeding RNAi. Bars represent the mean frequency (\pm SEM) of animals showing each phenotype from several independent experiments.
 (E) Quantification of the frequency of indicated mutant animals showing the Unc phenotype under *unc-15* feeding RNAi. Bars represent the mean frequency (\pm SEM) of animals showing each phenotype from several independent experiments.
 (F) FYVE-associated vesicle size (mean \pm SEM) in wild-type day-1 adult hermaphrodites that were pseudocoelomically injected with DMSO or 1 μ M TPEN. Data from wild-type and *zipt-9(0)* day-1 adult hermaphrodites without injection are also shown as a comparison. For each condition, images from more than 20 coelomocytes were analyzed.

any reduction in the suppressive effect of the *zipt-9* mutation, indicating that the impact of zinc is specific. These findings suggest that zinc has a specific repressive effect on RNAi, which becomes apparent in situations where systemic RNAi is not effective. The observation that the repressive effect of the *zipt-9* mutation was weakened by zinc implies the partial compensation by zinc transporters other than ZIPT-9. Nevertheless, this reduction was not complete, indicating that zinc transport via *zipt-9* is a crucial factor in RNAi.

DISCUSSION

ZIPT-9 plays a negative role in the regulation of RNAi activity

Here, we demonstrate negative regulation by ZIPT-9 in systemic RNAi. Our results provide the first example of Zn^{2+} and its transporter acting in the regulation of RNAi. We propose that ZIPT-9-dependent Zn^{2+} homeostasis, rather than regulation by overall cytosolic Zn^{2+} homeostasis, impacts RNAi activity regulation (Figure 8). Rescue experiments indicated that the zinc transporter activity of ZIPT-9 is required for enhanced RNAi and that the cytoplasmic Zn^{2+} levels in *zipt-9* mutant animals did not increase in response to transiently elevated dietary Zn^{2+} . These observations suggest that ZIPT-9 is involved in systemic RNAi through Zn^{2+} transport. In agreement with the results outlined above, the addition of Zn^{2+} but not of other metals enhanced the Rde phenotype in the *rsd-3* mutants. Comprehensive analysis of zinc transporter mutants revealed no involvement of zinc transporters other than ZIPT-9 under normal culture conditions, suggesting a specific function for ZIPT-9. However, the suppressive effect of the *zipt-9* mutation in *rsd-3* mutants was partially alleviated by the addition of Zn^{2+} , which suggests that other zinc transporters can compensate for ZIPT-9's function. Notably, we found that the *zipt-9* mutants showed undisturbed cytosolic Zn^{2+} levels under normal culture conditions. Regulation of Zn^{2+} -responsible genes at the transcriptional level is an important mechanism to maintain zinc homeostasis.^{2,35} Consistently, we found the repression of Zn^{2+} -responsible *mtl-1* expression in *zipt-9* mutant animals, suggesting that the mutants could be spared from a state of cytoplasmic Zn^{2+} deficiency by downregulating the expression of Zn^{2+} -responsive genes, including *mtl-1*. Some plasma membrane zinc transporters, such as ZRT1 and ZIP1, are endocytosed and inactivated in the presence of high extracellular zinc concentrations.^{36,37} Such transporters import zinc on the plasma membrane but undergo degradation quickly after entering the cell. In contrast, mammalian endomembrane-localized zinc transporters, such as ZIP9³⁸ and ZIP7,³⁹ are involved in the release of zinc from endomembrane organelles, such as the Golgi and endoplasmic reticulum, into the cytosol. Since ZIPT-9 predominantly localized to endosomes, we speculate that ZIPT-9, like ZIP9 and ZIP7, also releases zinc from endosomes into the cytosol after endocytosis. Thus, how zinc transporters and endocytosis coordinate to control cell physiology and RNAi activity is an important question for the future.

ZIPT-9 negatively regulates systemic RNAi via multiple mechanisms, possibly including the modulation of membrane trafficking

We found that ZIPT-9 negatively regulates at least the import of extracellular dsRNA. We propose that ZIPT-9 functions in systemic RNAi through multiple mechanisms, including through the modulation of endomembrane trafficking. Its regulation of endomembrane trafficking is supported by several observations. First, ZIPT-9 is mainly localized to late endosomes. Second, its mutants have defects in the distribution patterns of endomembrane organelle markers: loss of ZIPT-9 function seems likely to affect membrane trafficking from early and late endosomes to lysosomes. Third, its mutants suppress the Rde phenotype of loss of *sid-3*, *rsd-3*, and *sid-5*, which encode endomembrane proteins,^{12,14,15} while they exacerbate the Eri phenotype of *rrf-3* mutants. Previous studies have suggested both positive and negative roles of membrane trafficking in RNAi activity.^{10,11,16,21} Our data support a role for ZIPT-9 in trafficking from early and late endosomes to lysosomes. SEC-22¹⁶ and ARL-8¹¹ are the proteins involved in membrane trafficking from late endosomes and function as negative factors for systemic RNAi. Therefore, there might be some functional link between these molecules and ZIPT-9. However, the phenotypes of animals lacking these genes were distinctive from those lacking *zipt-9*: *sec-22* mutants never suppressed the Rde

Table 1. Loss of zinc transporters other than ZIPT-9 did not show RNAi-defective phenotype or RNAi-enhancing phenotype in *rsd-3(0)*

Type	gene name	mutant allele	<i>bli-3, pos-1</i> RNAi (single mutant)	<i>bli-3, pos-1</i> RNAi (double mutant with <i>rsd-3(0)</i>)
ZIP	<i>zipt-1</i> (F31C3.4)	<i>tm9689</i>	+	-
ZIP	<i>zipt-2.3</i> (Y54G9A.4)	<i>ok2094</i>	+	-
ZIP	<i>zipt-2.2</i> (F30B5.7)	<i>tm9681</i>	+	-
ZIP	<i>zipt-17</i> (C30H6.2)	<i>ok745</i>	+	-
ZIP	<i>zipt-7.1</i> (T28F3.3)	<i>ok971</i>	+	-
ZIP	<i>zipt-7.2</i> (H13N06.5)	<i>ok960^a</i>	+	not tested
ZIP	<i>zipt-15</i> (Y55F3BL.2)	<i>ok2160</i>	+	-
ZIP	<i>zipt-16</i> (T11F9.2)	<i>ok875</i>	+	-
ZIP	<i>zipt-9</i> (T01D3.5)	<i>tm9028, tm9416</i>	+	+
ZIP	<i>zipt-3</i> (C18A3.2)	<i>tm9694</i>	+	-
ZIP	<i>zipt-11</i> (F59A3.4)	<i>tm9668</i>	+	-
ZIP	<i>zipt-13</i> (C14H10.1)	<i>tm9696, tm9698^b</i>	+	-
ZIP	<i>zipt-2.1</i> (C06G8.3)	<i>tm9810</i>	+	-
ZIP	<i>zipt-2.4</i> (F55F8.9)	<i>tm9809</i>	+	-
ZnT	Y105E8A.3	<i>tm3941^a</i>	+	not tested
ZnT	<i>ttm-1</i> (Y39E4A.2)	<i>tm6576</i>	+	-
ZnT	<i>cdf-2</i> (T18D3.3)	<i>tm788</i>	+	-
ZnT	<i>toc-1</i> (ZC395.3)	<i>tm4492^a</i>	+	not tested
ZnT	Y71H2AM.9	<i>tm9680^b</i>	+	not tested
ZnT	R02F11.3	<i>tm9690</i>	+	-
ZnT	<i>cdf-1</i> (C15B12.7)	<i>n2527, tm9782^c</i>	+	-
ZnT	<i>sur-7</i> (F01G12.2)	<i>tm6523</i>	+	-
ZnT	F19C6.5	<i>tm9677</i>	+	-
ZnT	F41C6.7	<i>tm9671</i>	+	-
ZnT	ZK185.5	<i>tm9685</i>	+	-
ZnT	K07G5.5	<i>tm9669</i>	+	-
ZnT	PDB1.1	<i>tm2708</i>	+	-
ZnT	F56C9.3	<i>tm9687</i>	+	-

+: RNAi sensitive. -: RNAi resistance.

^aThe homozygous animals showed lethal or sterile phenotype. Progeny from the balanced heterozygous hermaphrodites were analyzed. Only *bli-3* RNAi in the single mutants was tested.

^bThe homozygous animals showed severe growth defect, and only *bli-3* RNAi in the single mutants was tested.

^cDifferent alleles from the single mutants (*tm9696* or *n2527*) was created using CRISPR/Cas9 in the *rsd-3(0)* background. Because these genes were on X chromosome where the *rsd-3* gene exists, we used this strategy, which was easier than to create recombinant with *rsd-3(0)* after obtaining the deletion allele.

phenotype caused by *sid-5* mutation,¹⁶ and *arl-8* weak alleles showed aberrant endogenous RNAi activity,¹¹ whereas our data suggested that *zipt-9(0)* suppressed the Rde phenotype caused by *sid-5* mutation, and ZIPT-9 acted in parallel with the endogenous RNAi pathway. These findings raised the possibility that systemic RNAi activity is regulated by multiple late endosome-related mechanisms. Consistently, previous studies have demonstrated both positive and negative roles of late endosomes in the regulation of non-coding RNAs.^{11,16,40–42} In a parallel or alternative scenario, ZIPT-9 may play a negative role on degradation of dsRNA in the lysosome. Such a function of ZIPT-9 could have an impact on systemic dsRNA levels, as intestinal expression of ZIPT-9 efficiently rescues the suppressor phenotype for RNAi defects in *rsd-3* mutants. The identification of factors regulated by Zn²⁺ transported through ZIPT-9 will help us understand how late endosome-related mechanisms negatively affect RNAi activity, although it could be challenging given the possibility of multiple target molecules. It should be noted that it is not actually proven in our study that there is a causal relationship between the membrane trafficking abnormality caused by *zipt-9*

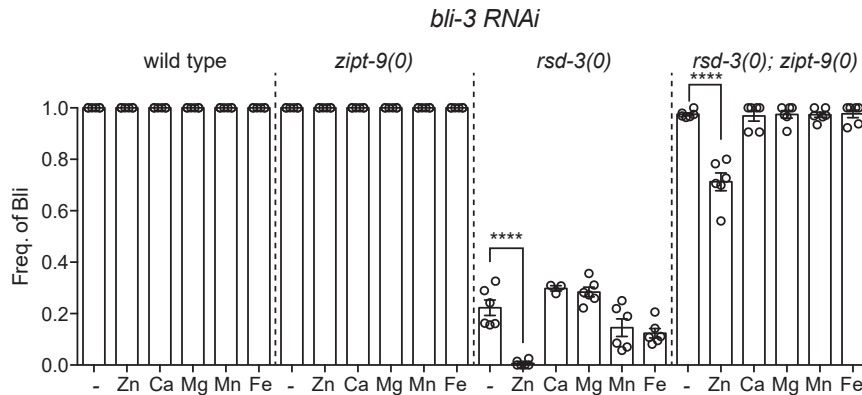


Figure 7. Effects of metals on *bli-3* feeding RNAi

Wild-type, *zipt-9(0)*, *rsd-3(0)*, and *rsd-3(0); zipt-9(0)* mutant animals were fed with bacteria producing dsRNA targeting the *bli-3* gene with no metal (–), or ZnSO₄ (Zn), CaCl₂ (Ca), MgSO₄ (Mg), MnCl₂ (Mn), or ferric ammonium citrate (Fe). Quantification of the frequency of indicated mutant animals showing the Bli phenotype under *bli-3* feeding RNAi. Bars represent the mean frequency (± SEM) of animals showing each phenotype from several independent experiments. ****p < 0.001.

mutations and enhanced RNAi activity. Injection of TPEN into the germline enhanced *pos-1* RNAi efficiency (Figure 6C). We examined if membrane trafficking was affected in this condition. However, we did not find any abnormalities in the size of the early endosome in the coelomocyte (Figure 6F). In this experiment in which coelomocytes from day 1 adults were examined, the abnormalities in the *zipt-9* mutant were weaker than those observed in L4. Thus, it is unclear whether an alteration of membrane trafficking status is the cause of the enhanced RNAi or whether alteration of cytosolic Zn²⁺ concentration changes membrane trafficking that affects RNAi efficacy.

Candidate effector molecules that can be regulated by ZIPT-9-dependent Zn²⁺

Previous studies have shown that ZIP9 functions as a membrane androgen receptor and stimulates G protein in croaker ovarian follicle cells.⁴³ However, ZIPT-9 seems to act through different mechanisms because ZIPT-9 is not localized to the plasma membrane in *C. elegans*, and neither steroid hormones nor G proteins have been shown to regulate systemic RNAi. Based on several lines of previous research, we speculate that Zn²⁺ transported through ZIPT-9 might affect the overall state of phosphoinositide phosphorylation as one of several mechanisms, which in turn modulates endomembrane trafficking and the activity of systemic RNAi. A previous study demonstrated that ZIP9 has an inhibitory effect on protein tyrosine phosphatase (PTPase) activity in DT40 cells.³⁸ The kinases that were shown to be involved in systemic RNAi were SID-3¹² and VPS-34,¹⁰ which encode an Ack tyrosine kinase and a PI3 kinase, respectively. The fact that loss of *zipt-9* results in an opposite phenotype to that of *sid-3* excludes the possibility that an unidentified PTPase that is antagonistic to SID-3 is the target of Zn²⁺ transported by ZIPT-9. On the other hand,

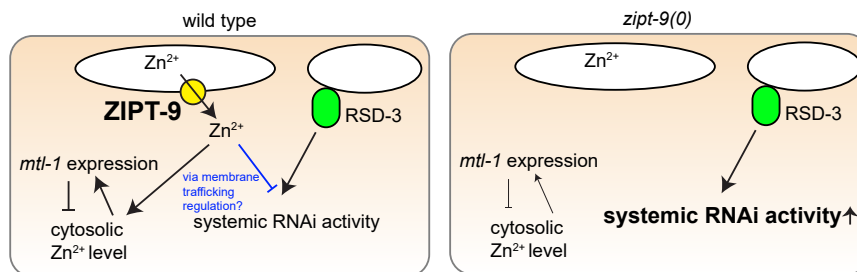


Figure 8. Model for regulation of systemic RNAi by ZIPT-9

ZIPT-9 imports Zn²⁺ from endosomes, and loss of ZIPT-9 results in a decrease in Zn²⁺ import, which leads to downregulation of the expression of the zinc responsible genes including *mtl-1* and, in turn, this response sustains entire cytosolic Zn²⁺ levels. Local Zn²⁺ around endosomal vesicles, which are transported by ZIPT-9, rather than entire cytosolic Zn²⁺ levels antagonistically modulates systemic RNAi activity with endomembrane molecules including RSD-3. This modulation may include the regulation of membrane trafficking from early and late endosomes to lysosomes.

some phosphoinositide phosphatases, which share several structural features of PTPases⁴⁴ and play crucial roles in vesicle trafficking, might directly or indirectly contribute to generating phosphatidylinositol 3-phosphate (PI3P), which is synthesized by VPS-34 and be one of the targets of Zn^{2+} transported through ZIPT-9. Interestingly, *zipt-9(0)* mutants also showed synthetic growth defects with *ipp-5(0)* mutants in which IP_3 signaling was activated (Figure 5E). Although this genetic interaction suggested that ZIPT-9 and IPP-5 function in different processes to enable larval growth, it also provided the possibility of a potential indirect link between ZIPT-9 and the production of IP_3 , which is derived from one of the phosphoinositides, PI(4,5) P_2 . In addition, recently, a reduction in ZIPT-9 function by RNAi was shown to induce DAF-16 nuclear localization, which could be triggered by a reduction in PI(3,4,5) P_3 .⁴⁵ However, to our knowledge, whether Zn^{2+} inhibits the activity of phosphoinositide phosphatases has not been studied. Although the lethal phenotype of most loss-of-function mutants for phosphoinositide modification enzyme genes such as *vps-34*, makes the analysis difficult and some alternative mechanisms of ZIPT-9 and Zn^{2+} functions are possible, understanding whether *zipt-9* genetically interacts with genes involved in phosphoinositide modification in the systemic RNAi phenotype might uncover how ZIPT-9 modulates the efficiency of systemic RNAi.

Because functional RNAs can spread throughout the whole body in organisms other than *C. elegans*, identifying factors involved in the negative regulation of systemic RNAi in *C. elegans* might generally contribute to efficient exo-RNA delivery. Accordingly, our study opens the possibility that optimization of local Zn^{2+} homeostasis around endosomal vesicles could change the efficiency of systemic functional RNA delivery in other model organisms, as well as insect pests and humans.

Limitations of the study

The zinc exporter CDF-1/ZnT1 has been shown to activate Ras signaling by removing Zn^{2+} from Raf-1 on the plasma membrane,^{46,47} suggesting the possibility that modulation of Zn^{2+} levels by zinc transporters localized to a specific subcellular compartment might contribute to local regulation of zinc-dependent proteins. In a similar way, ZIPT-9 could not only play a role in Zn^{2+} supplementation throughout the entire cytosol but could also have the ability to transport Zn^{2+} to a special subcellular compartment where zinc-dependent dsRNA import or RNAi machinery exists. However, we were not able to detect any subcellular changes in Zn^{2+} levels using the FRET sensor that we used. It will be important to determine exactly where Zn^{2+} is transported by ZIPT-9 at the subcellular level in future studies.

STAR★METHODS

Detailed methods are provided in the online version of this paper and include the following:

- KEY RESOURCES TABLE
- RESOURCE AVAILABILITY
 - Lead contact
 - Materials availability
 - Data and code availability
- EXPERIMENTAL MODEL AND STUDY PARTICIPANT DETAILS
- METHOD DETAILS
 - DNA preparation for injection
 - Mutagenesis screens
 - CRISPR/Cas9-mediated genome editing
 - Quantitative PCR
 - Analysis of *Pmtl-1::gfp*
 - Analysis of FRET-based Zn^{2+} sensor ZapCY2
 - Imaging
- QUANTIFICATION AND STATISTICAL ANALYSIS

SUPPLEMENTAL INFORMATION

Supplemental information can be found online at <https://doi.org/10.1016/j.isci.2023.106930>.

ACKNOWLEDGMENTS

We thank the Mitani lab members for their support and the Medical Research Institute (MRI) of Tokyo Women's Medical University for undertaking confocal microscope. Some strains were provided by the

CGC, which is funded by NIH Office of Research Infrastructure Programs (P40 OD010440). Some of the plasmids were provided by the Addgene. This work was supported by Technology of Japan Grants-in Aid for Scientific Research to K.D. (20K06561) and S.M. (20H03422), and a grant from the Takeda Science Foundation.

AUTHOR CONTRIBUTIONS

K.D.: Writing - original draft, Funding acquisition, Investigation, R.I.: Writing - review & editing, Conceptualization, Y.S.: Writing - review & editing, Investigation, K.Y.: Writing - review & editing, Conceptualization, S.M.: Writing - review & editing, Conceptualization, Funding acquisition.

DECLARATION OF INTERESTS

The authors declare no competing interests.

Received: February 17, 2023

Revised: April 18, 2023

Accepted: May 16, 2023

Published: May 19, 2023

REFERENCES

- Andreini, C., Banci, L., Bertini, I., and Rosato, A. (2006). Counting the zinc-proteins encoded in the human genome. *J. Proteome Res.* 5, 196–201. <https://doi.org/10.1021/pr050361j>.
- Fukada, T., and Kambe, T. (2011). Molecular and genetic features of zinc transporters in physiology and pathogenesis. *Metallomics* 3, 662–674. <https://doi.org/10.1039/c1mt00011j>.
- Kambe, T., Tsuji, T., Hashimoto, A., and Itsumura, N. (2015). The physiological, biochemical, and molecular roles of zinc transporters in zinc homeostasis and metabolism. *Physiol. Rev.* 95, 749–784. <https://doi.org/10.1152/physrev.00035.2014>.
- Hara, T., Yoshigai, E., Ohashi, T., and Fukada, T. (2022). Zinc transporters as potential therapeutic targets: an updated review. *J. Pharmacol. Sci.* 148, 221–228. <https://doi.org/10.1016/j.jpsh.2021.11.007>.
- Fire, A., Xu, S., Montgomery, M.K., Kostas, S.A., Driver, S.E., and Mello, C.C. (1998). Potent and specific genetic interference by double-stranded RNA in *Caenorhabditis elegans*. *Nature* 391, 806–811. <https://doi.org/10.1038/35888>.
- Jose, A.M. (2015). Movement of regulatory RNA between animal cells. *Genesis* 53, 395–416. <https://doi.org/10.1002/dvg.22871>.
- Winston, W.M., Molodowitch, C., and Hunter, C.P. (2002). Systemic RNAi in *C. elegans* requires the putative transmembrane protein SID-1. *Science* 295, 2456–2459. <https://doi.org/10.1126/science.1068836>.
- Feinberg, E.H., and Hunter, C.P. (2003). Transport of dsRNA into cells by the transmembrane protein SID-1. *Science* 301, 1545–1547. <https://doi.org/10.1126/science.1087117>.
- Nguyen, T.A., Smith, B.R.C., Tate, M.D., Belz, G.T., Barrios, M.H., Elgass, K.D., Weisman, A.S., Baker, P.J., Preston, S.P., Whitehead, L., et al. (2017). SIDT2 transports extracellular dsRNA into the cytoplasm for innate immune recognition. *Immunity* 47, 498–509. <https://doi.org/10.1016/j.immuni.2017.08.007>.
- Saleh, M.C., van Rij, R.P., Hekele, A., Gillis, A., Foley, E., O'Farrell, P.H., and Andino, R. (2006). The endocytic pathway mediates cell entry of dsRNA to induce RNAi silencing. *Nat. Cell Biol.* 8, 793–802. <https://doi.org/10.1038/ncb1439>.
- Fischer, S.E.J., Pan, Q., Breen, P.C., Qi, Y., Shi, Z., Zhang, C., and Ruvkun, G. (2013). Multiple small RNA pathways regulate the silencing of repeated and foreign genes in *C. elegans*. *Genes Dev.* 27, 2678–2695. <https://doi.org/10.1101/gad.233254.113>.
- Jose, A.M., Kim, Y.A., Leal-Ekman, S., and Hunter, C.P. (2012). Conserved tyrosine kinase promotes the import of silencing RNA into *Caenorhabditis elegans* cells. *Proc. Natl. Acad. Sci. USA* 109, 14520–14525. <https://doi.org/10.1073/pnas.1201153109>.
- Tijsterman, M., May, R.C., Simmer, F., Okihara, K.L., and Plasterk, R.H.A. (2004). Genes required for systemic RNA interference in *Caenorhabditis elegans*. *Curr. Biol.* 14, 111–116.
- Imae, R., Dejima, K., Kage-Nakadai, E., Arai, H., and Mitani, S. (2016). Endomembrane-associated RSD-3 is important for RNAi induced by extracellular silencing RNA in both somatic and germ cells of *Caenorhabditis elegans*. *Sci. Rep.* 6, 28198. <https://doi.org/10.1038/srep28198>.
- Hinas, A., Wright, A.J., and Hunter, C.P. (2012). SID-5 is an endosome-associated protein required for efficient systemic RNAi in *C. elegans*. *Curr. Biol.* 22, 1938–1943. <https://doi.org/10.1016/j.cub.2012.08.020>.
- Zhao, Y., Holmgren, B.T., and Hinas, A. (2017). The conserved SNARE SEC-22 localizes to late endosomes and negatively regulates RNA interference in *Caenorhabditis elegans*. *Rna* 23, 297–307. <https://doi.org/10.1261/ma.058438.116>.
- Nagy, A.I., Vázquez-Manrique, R.P., Lopez, M., Christov, C.P., Sequedo, M.D., Herzog, M., Herlihy, A.E., Bodak, M., Gatsi, R., and Baylis, H.A. (2015). IP3 signalling regulates exogenous RNAi in *Caenorhabditis elegans*. *EMBO Rep.* 16, 341–350. <https://doi.org/10.15252/embr.201439585>.
- Timmons, L., and Fire, A. (1998). Specific interference by ingested dsRNA. *Nature* 395, 854. <https://doi.org/10.1038/27579>.
- Winston, W.M., Sutherlin, M., Wright, A.J., Feinberg, E.H., and Hunter, C.P. (2007). *Caenorhabditis elegans* SID-2 is required for environmental RNA interference. *Proc. Natl. Acad. Sci. USA* 104, 10565–10570. <https://doi.org/10.1073/pnas.0611282104>.
- McEwan, D.L., Weisman, A.S., and Hunter, C.P. (2012). Uptake of extracellular double-stranded RNA by SID-2. *Mol. Cell* 47, 746–754. <https://doi.org/10.1016/j.molcel.2012.07.014>.
- Gao, J., Zhao, L., Luo, Q., Liu, S., Lin, Z., Wang, P., Fu, X., Chen, J., Zhang, H., Lin, L., and Shi, A. (2020). An EHBP-1-SID-3-DYN-1 axis promotes membranous tubule fission during endocytic recycling. *PLoS Genet.* 16, e1008763. <https://doi.org/10.1371/journal.pgen.1008763>.
- Kennedy, S., Wang, D., and Ruvkun, G. (2004). A conserved siRNA-degrading RNase negatively regulates RNA interference in *C. elegans*. *Nature* 427, 645–649. <https://doi.org/10.1038/nature02302>.
- Duchaine, T.F., Wohlschlegel, J.A., Kennedy, S., Bei, Y., Conte, D., Jr., Pang, K., Brownell, D.R., Harding, S., Mitani, S., Ruvkun, G., et al. (2006). Functional proteomics reveals the biochemical niche of *C. elegans* DCR-1 in multiple small-RNA-mediated pathways. *Cell* 124, 343–354. <https://doi.org/10.1016/j.cell.2005.11.036>.
- Conine, C.C., Batista, P.J., Gu, W., Claycomb, J.M., Chaves, D.A., Shirayama, M., and Mello, C.C. (2010). Argonautes ALG-3 and ALG-4 are required for spermatogenesis-specific 26G-RNAs and thermotolerant sperm in *Caenorhabditis elegans*. *Proc. Natl. Acad.*

- Sci. USA 107, 3588–3593. <https://doi.org/10.1073/pnas.0911685107>.
25. Kim, Y.J., Maizel, A., and Chen, X. (2014). Traffic into silence: endomembranes and post-transcriptional RNA silencing. *EMBO J.* 33, 968–980. <https://doi.org/10.1002/embj.201387262>.
26. Friedland, A.E., Tzur, Y.B., Esvelt, K.M., Colaiácovo, M.P., Church, G.M., and Calarco, J.A. (2013). Heritable genome editing in *C. elegans* via a CRISPR-Cas9 system. *Nat. Methods* 10, 741–743. <https://doi.org/10.1038/nmeth.2532>.
27. Dickinson, D.J., Ward, J.D., Reiner, D.J., and Goldstein, B. (2013). Engineering the *Caenorhabditis elegans* genome using Cas9-triggered homologous recombination. *Nat. Methods* 10, 1028–1034. <https://doi.org/10.1038/nmeth.2641>.
28. Roh, H.C., Collier, S., Deshmukh, K., Guthrie, J., Robertson, J.D., and Kornfeld, K. (2013). *ttm-1* encodes CDF transporters that excrete zinc from intestinal cells of *C. elegans* and act in a parallel negative feedback circuit that promotes homeostasis. *PLoS Genet.* 9, e1003522. <https://doi.org/10.1371/journal.pgen.1003522>.
29. Qin, Y., Miranda, J.G., Stoddard, C.I., Dean, K.M., Galati, D.F., and Palmer, A.E. (2013). Direct comparison of a genetically encoded sensor and small molecule indicator: implications for quantification of cytosolic Zn(2+). *ACS Chem. Biol.* 8, 2366–2371. <https://doi.org/10.1021/cb4003859>.
30. Simmer, F., Tijsterman, M., Parrish, S., Koushika, S.P., Nonet, M.L., Fire, A., Ahringer, J., and Plasterk, R.H.A. (2002). Loss of the putative RNA-directed RNA polymerase RRF-3 makes *C. elegans* hypersensitive to RNAi. *Curr. Biol.* 12, 1317–1319. [https://doi.org/10.1016/s0960-9822\(02\)01041-2](https://doi.org/10.1016/s0960-9822(02)01041-2).
31. Matsuura, W., Yamazaki, T., Yamaguchi-Iwai, Y., Masuda, S., Nagao, M., Andrews, G.K., and Kambe, T. (2009). SLC39A9 (ZIP9) regulates zinc homeostasis in the secretory pathway: characterization of the ZIP subfamily I protein in vertebrate cells. *Biosci. Biotechnol. Biochem.* 73, 1142–1148. <https://doi.org/10.1271/bbb.80910>.
32. Qiu, Y., Gao, Y., Yu, D., Zhong, L., Cai, W., Ji, J., Geng, F., Tang, G., Zhang, H., Cao, J., et al. (2020). Genome-wide analysis reveals zinc transporter ZIP9 regulated by DNA methylation promotes radiation-induced skin fibrosis via the TGF-beta signaling pathway. *J. Invest. Dermatol.* 140, 94–102.e7. <https://doi.org/10.1016/j.jid.2019.04.027>.
33. Fares, H., and Greenwald, I. (2001). Genetic analysis of endocytosis in *Caenorhabditis elegans*: coelomocyte uptake defective mutants. *Genetics* 159, 133–145. <https://doi.org/10.1093/genetics/159.1.133>.
34. Raman, P., Zaghbab, S.M., Traver, E.C., and Jose, A.M. (2017). The double-stranded RNA binding protein RDE-4 can act cell autonomously during feeding RNAi in *C. elegans*. *Nucleic Acids Res.* 45, 8463–8473. <https://doi.org/10.1093/nar/gkx484>.
35. Roh, H.C., Dimitrov, I., Deshmukh, K., Zhao, G., Warnhoff, K., Cabrera, D., Tsai, W., and Kornfeld, K. (2015). A modular system of DNA enhancer elements mediates tissue-specific activation of transcription by high dietary zinc in *C. elegans*. *Nucleic Acids Res.* 43, 803–816. <https://doi.org/10.1093/nar/gku1360>.
36. Wang, F., Dufner-Beattie, J., Kim, B.E., Petris, M.J., Andrews, G., and Eide, D.J. (2004). Zinc-stimulated endocytosis controls activity of the mouse ZIP1 and ZIP3 zinc uptake transporters. *J. Biol. Chem.* 279, 24631–24639. <https://doi.org/10.1074/jbc.M400680200>.
37. Gitan, R.S., Luo, H., Rodgers, J., Broderius, M., and Eide, D. (1998). Zinc-induced inactivation of the yeast ZRT1 zinc transporter occurs through endocytosis and vacuolar degradation. *J. Biol. Chem.* 273, 28617–28624. <https://doi.org/10.1074/jbc.273.44.28617>.
38. Taniguchi, M., Fukunaka, A., Hagihara, M., Watanabe, K., Kamino, S., Kambe, T., Enomoto, S., and Hiromura, M. (2013). Essential role of the zinc transporter ZIP9/SLC39A9 in regulating the activations of Akt and Erk in B-cell receptor signaling pathway in DT40 cells. *PLoS One* 8, e58022. <https://doi.org/10.1371/journal.pone.0058022>.
39. Taylor, K.M., Morgan, H.E., Johnson, A., and Nicholson, R.I. (2004). Structure-function analysis of HKE4, a member of the new LIV-1 subfamily of zinc transporters. *Biochem. J.* 377, 131–139. <https://doi.org/10.1042/BJ20031183>.
40. Gibbings, D.J., Ciaudo, C., Erhardt, M., and Voynet, O. (2009). Multivesicular bodies associate with components of miRNA effector complexes and modulate miRNA activity. *Nat. Cell Biol.* 11, 1143–1149. <https://doi.org/10.1038/ncb1929>.
41. Lee, Y.S., Pressman, S., Andress, A.P., Kim, K., White, J.L., Cassidy, J.J., Li, X., Lubell, K., Lim, D.H., Cho, I.S., et al. (2009). Silencing by small RNAs is linked to endosomal trafficking. *Nat. Cell Biol.* 11, 1150–1156. <https://doi.org/10.1038/ncb1930>.
42. Wang, H., Tam, Y.Y.C., Chen, S., Zaifman, J., van der Meel, R., Ciufolini, M.A., and Cullis, P.R. (2016). The niemann-pick C1 inhibitor NP3.47 enhances gene silencing potency of lipid nanoparticles containing siRNA. *Mol. Ther.* 24, 2100–2108. <https://doi.org/10.1038/mt.2016.179>.
43. Converse, A., Zhang, C., and Thomas, P. (2017). Membrane androgen receptor ZIP9 induces croaker ovarian cell apoptosis via stimulatory G protein alpha subunit and MAP kinase signaling. *Endocrinology* 158, 3015–3029. <https://doi.org/10.1210/en.2017-00087>.
44. Hsu, F., and Mao, Y. (2015). The structure of phosphoinositide phosphatases: Insights into substrate specificity and catalysis. *Biochim. Biophys. Acta* 1851, 698–710. <https://doi.org/10.1016/j.bbali.2014.09.015>.
45. Novakovic, S., Molesworth, L.W., Gourley, T.E., Boag, P.R., and Davis, G.M. (2020). Zinc transporters maintain longevity by influencing insulin/IGF-1 activity in *Caenorhabditis elegans*. *FEBS Lett.* 594, 1424–1432. <https://doi.org/10.1002/1873-3468.13725>.
46. Jirakulaporn, T., and Muslin, A.J. (2004). Cation diffusion facilitator proteins modulate Raf-1 activity. *J. Biol. Chem.* 279, 27807–27815. <https://doi.org/10.1074/jbc.M401210200>.
47. Bruinsma, J.J., Jirakulaporn, T., Muslin, A.J., and Kornfeld, K. (2002). Zinc ions and cation diffusion facilitator proteins regulate Ras-mediated signaling. *Dev. Cell* 2, 567–578.
48. Timmons, L., Court, D.L., and Fire, A. (2001). Ingestion of bacterially expressed dsRNAs can produce specific and potent genetic interference in *Caenorhabditis elegans*. *Gene* 263, 103–112.
49. Treusch, S., Knuth, S., Slaugenhaupt, S.A., Goldin, E., Grant, B.D., and Fares, H. (2004). *Caenorhabditis elegans* functional orthologue of human protein h-mucolipin-1 is required for lysosome biogenesis. *Proc. Natl. Acad. Sci. USA* 101, 4483–4488.
50. Dang, H., Li, Z., Skolnik, E.Y., and Fares, H. (2004). Disease-related myotubularin function in endocytic traffic in *Caenorhabditis elegans*. *Mol. Biol. Cell* 15, 189–196.
51. Schneider, C.A., Rasband, W.S., and Eliceiri, K.W. (2012). NIH Image to ImageJ: 25 years of image analysis. *Nat. Methods* 9, 671–675.
52. Brenner, S. (1974). The genetics of *Caenorhabditis elegans*. *Genetics* 77, 71–94.
53. Zuryn, S., Le Gras, S., Jamet, K., and Jarriault, S. (2010). A strategy for direct mapping and identification of mutations by whole-genome sequencing. *Genetics* 186, 427–430. <https://doi.org/10.1534/genetics.110.119230>.
54. Suehiro, Y., Yoshina, S., Motohashi, T., Iwata, S., Dejima, K., and Mitani, S. (2021). Efficient collection of a large number of mutations by mutagenesis of DNA damage response defective animals. *Sci. Rep.* 11, 7630. <https://doi.org/10.1038/s41598-021-87226-7>.
55. Dejima, K., Hori, S., Iwata, S., Suehiro, Y., Yoshina, S., Motohashi, T., and Mitani, S. (2018). An aneuploidy-free and structurally defined balancer chromosome toolkit for *Caenorhabditis elegans*. *Cell Rep.* 22, 232–241. <https://doi.org/10.1016/j.celrep.2017.12.024>.
56. Edgley, M.L., Baillie, D.L., Riddle, D.L., and Rose, A.M. (2006). Genetic Balancers (WormBook), pp. 1–32. <https://doi.org/10.1895/wormbook.1.89.1>.

STAR★METHODS

KEY RESOURCES TABLE

REAGENT or RESOURCE	SOURCE	IDENTIFIER
Bacterial and virus strains		
OP50-1	Chalfie lab	N/A
HT115	CGC	N/A
Chemicals, peptides, and recombinant proteins		
isopropyl β-D-1-thiogalactopyranoside (IPTG)	Sigma Aldrich	I6758
TRIzol	Invitrogen	Cat: 15596026
SuperScript IV Reverse Transcriptase	Invitrogen	Cat: 18090010
TPEN (N,N,N',N'-Tetrakis(2-pyridylmethyl) ethylenediamine)	FUJIFILM Wako	340-05411
Critical commercial assays		
Power™ SYBR™ Green Master Mix	Applied Biosystems	Cat: 4368702
Deposited data		
WGS data (tm9006)	This paper	NCBI Trace Archive: SRR23325556
WGS data (tm9028; tm9006)	This paper	NCBI Trace Archive: SRR23325555
Experimental models: Organisms/strains		
<i>C. elegans</i> wild type	CGC	N2
ccls4251[(pSAK2) myo-3p::GFP::LacZ::NLS + (pSAK4) myo-3p::mitochondrial GFP + dpy-20(+)] [(pSAK2) myo-3p::GFP::LacZ::NLS + (pSAK4) myo-3p::mitochondrial GFP + dpy-20(+)] l; rsd-3(tm9006) X; tmls964[Pmyo-3::mCherry]	This study and CGC, ^{5,14}	FX15035
ccls4251[(pSAK2) myo-3p::GFP::LacZ::NLS + (pSAK4) myo-3p::mitochondrial GFP + dpy-20(+)] 1[(pSAK2) myo-3p::GFP::LacZ::NLS + (pSAK4) myo-3p::mitochondrial GFP + dpy-20(+)] l; zip1-9(tm9028) V; rsd-3(tm9006) X; tmls964[Pmyo-3::mCherry]	This study and CGC, ^{5,14}	FX16921
ccls4251[(pSAK2) myo-3p::GFP::LacZ::NLS + (pSAK4) myo-3p::mitochondrial GFP + dpy-20(+)] 1[(pSAK2) myo-3p::GFP::LacZ::NLS + (pSAK4) myo-3p::mitochondrial GFP + dpy-20(+)] l; zip1-9(tm9028) V; rsd-3(tm9006) X; tmls964[Pmyo-3::mCherry]	This study and CGC, ^{5,14}	FX17549
ccls4251[(pSAK2) myo-3p::GFP::LacZ::NLS + (pSAK4) myo-3p::mitochondrial GFP + dpy-20(+)] 1[(pSAK2) myo-3p::GFP::LacZ::NLS + (pSAK4) myo-3p::mitochondrial GFP + dpy-20(+)] l; zip1-9(tm9028) V; rsd-3(tm9006) X; tmEx4305[zip1-9(+); Pmyo-2::mCherry]	This study and CGC, ^{5,14}	FX17549
ccls4251[(pSAK2) myo-3p::GFP::LacZ::NLS + (pSAK4) myo-3p::mitochondrial GFP + dpy-20(+)] l; zip1-9(tm9028) V; rsd-3(tm9006) X; tmEx4306[zip1-9(+); Pmyo-2::mCherry]	This study and CGC, ^{5,14}	FX18070

(Continued on next page)

Continued

REAGENT or RESOURCE	SOURCE	IDENTIFIER
ccls4251[(pSAK2) myo-3p::GFP::LacZ::NLS + (pSAK4) myo-3p::mitochondrial GFP + dpy-20(+)] I; zipt-9(tm9028) V; rsd-3(tm9006) X; tmEx4306[zipt-9(+); Pmyo-2::mCherry]	This study and CGC, ^{5,14}	FX18071
ccls4251[(pSAK2) myo-3p::GFP::LacZ::NLS + (pSAK4) myo-3p::mitochondrial GFP + dpy-20(+)] I; zipt-9(tm9028) V; rsd-3(tm9006) X; tmEx4307[zipt-9(+); Pmyo-2::mCherry]	This study and CGC, ^{5,14}	FX18072
ccls4251[(pSAK2) myo-3p::GFP::LacZ::NLS + (pSAK4) myo-3p::mitochondrial GFP + dpy-20(+)] I; zipt-9(tm9028) V; rsd-3(tm9006) X; tmEx4302[ttr-21(+); Pmyo-2::mCherry]	This study and CGC, ^{5,14}	FX18067
ccls4251[(pSAK2) myo-3p::GFP::LacZ::NLS + (pSAK4) myo-3p::mitochondrial GFP + dpy-20(+)] I; zipt-9(tm9028) V; rsd-3(tm9006) X; tmEx4303[ttr-21(+); Pmyo-2::mCherry]	This study and CGC, ^{5,14}	FX18068
ccls4251[(pSAK2) myo-3p::GFP::LacZ::NLS + (pSAK4) myo-3p::mitochondrial GFP + dpy-20(+)] I; zipt-9(tm9028) V; rsd-3(tm9006) X; tmEx4304[ttr-21(+); Pmyo-2::mCherry]	This study and CGC, ^{5,14}	FX18069
ccls4251[(pSAK2) myo-3p::GFP::LacZ::NLS + (pSAK4) myo-3p::mitochondrial GFP + dpy-20(+)] I; zipt-9(tm9028) V; rsd-3(tm9006) X; tmEx4279[ccz-1(+); Pmyo-2::mCherry]	This study and CGC, ^{5,14}	FX18001
ccls4251[(pSAK2) myo-3p::GFP::LacZ::NLS + (pSAK4) myo-3p::mitochondrial GFP + dpy-20(+)] I; zipt-9(tm9028) V; rsd-3(tm9006) X; tmEx4280[ccz-1(+); Pmyo-2::mCherry]	This study and CGC, ^{5,14}	FX18002
ccls4251[(pSAK2) myo-3p::GFP::LacZ::NLS + (pSAK4) myo-3p::mitochondrial GFP + dpy-20(+)] I; zipt-9(tm9028) V; rsd-3(tm9006) X; tmEx4281[ccz-1(+); Pmyo-2::mCherry]	This study and CGC, ^{5,14}	FX18003
ccls4251[(pSAK2) myo-3p::GFP::LacZ::NLS + (pSAK4) myo-3p::mitochondrial GFP + dpy-20(+)] I; zipt-9(tm9028) V; rsd-3(tm9006) X; tmEx4282[ccz-1(+); Pmyo-2::mCherry]	This study and CGC, ^{5,14}	FX18004
zipt-9(tm9416) V	This study	FX18616
zipt-9(tm9416) V; rsd-3(tm9006) X; tmEx4575 [Pzipt-9::hZIP9; Pmyo-2::mCherry]	This study and ¹⁴	FX18727
zipt-9(tm9416) V; rsd-3(tm9006) X; tmEx4576 [Pzipt-9::hZIP9; Pmyo-2::mCherry]	This study and ¹⁴	FX18728
zipt-9(tm9416) V; rsd-3(tm9006) X; tmEx4600 [Pzipt-9::hZIP9; Pmyo-2::mCherry]	This study and ¹⁴	FX19551
zipt-9(tm9416) V; rsd-3(tm9006) X; tmEx4601 [Pzipt-9::hZIP9; Pmyo-2::mCherry]	This study and ¹⁴	FX19552
zipt-9(tm9416) V; rsd-3(tm9006) X; tmEx4596 [Pzipt-9::zipt-9::egfp; Pmyo-2::mCherry]	This study and ¹⁴	FX19549
zipt-9(tm9416) V; rsd-3(tm9006) X; tmEx4597 [Pzipt-9::zipt-9::egfp; Pmyo-2::mCherry]	This study and ¹⁴	FX19556

(Continued on next page)

Continued

REAGENT or RESOURCE	SOURCE	IDENTIFIER
zipt-9(tm9416) V; rsd-3(tm9006) X; tmEx4598 [Pzipt-9::zipt-9::egfp; Pmyo-2::mCherry]	This study and ¹⁴	FX19550
zipt-9(tm9416) V; rsd-3(tm9006) X; tmEx4591 [Pzipt-9::zipt-9::tagRFP; Pmyo-2::mCherry]	This study and ¹⁴	FX19541
zipt-9(tm9416) V; rsd-3(tm9006) X; tmEx4592 [Pzipt-9::zipt-9::tagRFP; Pmyo-2::mCherry]	This study and ¹⁴	FX19542
zipt-9(tm9416) V; rsd-3(tm9006) X; tmEx4593 [Pzipt-9::zipt-9::tagRFP; Pmyo-2::mCherry]	This study and ¹⁴	FX19543
tmEx4662[Pmtl-1::gfp; Pmyo-2::mCherry]	This study	FX19618
zipt-9(tm9416) V; tmEx4662[Pmtl-1::gfp; Pmyo-2::mCherry]	This study	FX30087
rsd-3(tm9006) X; tmEx4662[Pmtl-1::gfp; Pmyo- 2::mCherry]	This study	FX19799
tmEx4758[Pvha-6::NES::ZapCY2]	This study	FX30360
zipt-9(tm9416) V; tmEx4758[Pvha- 6::NES::ZapCY2]	This study	FX30695
zipt-9(tm9416) V; rsd-3(tm9006) X; tmEx4683 [Pvha-6::zipt-9::GFP, Pmyo-2::mCherry]	This study and ¹⁴	FX30081
zipt-9(tm9416) V; rsd-3(tm9006) X; tmEx4684 [Pvha-6::zipt-9::GFP, Pmyo-2::mCherry]	This study and ¹⁴	FX30078
zipt-9(tm9416) V; rsd-3(tm9006) X; tmEx4634 [Pvha-6::zipt-9(H217A)::GFP, Pmyo- 2::mCherry]	This study and ¹⁴	FX19566
zipt-9(tm9416) V; rsd-3(tm9006) X; tmEx4635 [Pvha-6::zipt-9(H217A)::GFP, Pmyo- 2::mCherry]	This study and ¹⁴	FX19567
zipt-9(tm9416) V; rsd-3(tm9006) X; tmEx4831 [Pvha-6::zipt-9(H247A)::GFP, Pmyo- 2::mCherry]	This study and ¹⁴	FX30584
zipt-9(tm9416) V; rsd-3(tm9006) X; tmEx4832 [Pvha-6::zipt-9(H247A)::GFP, Pmyo- 2::mCherry]	This study and ¹⁴	FX30585
zipt-9(tm9416) V; rsd-3(tm9006) X; tmEx4794 [Pvha-6::zipt-9(H217A, H247A)::GFP, Pmyo- 2::mCherry]	This study and ¹⁴	FX30440
zipt-9(tm9416) V; rsd-3(tm9006) X; tmEx4796 [Pvha-6::zipt-9(H217A, H247A)::GFP, Pmyo- 2::mCherry]	This study and ¹⁴	FX30442
eri-1(mg366) IV	CGC and ²²	GR1373
rff-3(tm6937) II	NBRP	FX06937
rff-3(tm6937) II; zipt-9(tm9416) V	This study and NBRP	FX31842
tmEx4437[Pzipt-9::zipt-9::tagRFP; Plin-44::gfp]	This study	FX19049
pwls69[vha6p::GFP::rab-11 + unc-119(+)] X; tmEx4437[Pzipt-9::zipt-9::tagRFP; Plin-44::gfp]	This study and CGC, ⁴⁸	FX18646
pwls50[Imp-1::GFP + Cbr-unc-119(+)]; tmEx4437[Pzipt-9::zipt-9::tagRFP; Plin-44::gfp]	This study and CGC, ⁴⁹	FX19041
pwls72[vha-6p::GFP::rab-5 + Cbr-unc-119(+)] II; tmEx4437[Pzipt-9::zipt-9::tagRFP; Plin- 44::gfp]	This study and CGC, ⁴⁸	FX19042

(Continued on next page)

Continued

REAGENT or RESOURCE	SOURCE	IDENTIFIER
<i>pwls503</i> [<i>vha-6p::mans::GFP + Cbr-unc-119(+)</i>]; <i>tmEx4440</i> [<i>Pzipt-9::zipt-9::tagRFP; Plin-44::gfp</i>]	This study and CGC, ⁴⁸	FX18649
<i>pwls170</i> [<i>vha6p::GFP::rab-7 + Cbr-unc-119(+)</i>]; <i>tmEx4438</i> [<i>Pzipt-9::zipt-9::tagRFP; Plin-44::gfp</i>]	This study and CGC, ⁴⁸	FX18647
<i>unc-119(ed3) III</i> ; <i>cdls85</i> [<i>pcc1::2xFYVE::GFP + myo-2p::GFP + unc-119(+)</i>]	CGC and ⁵⁰	NP941
<i>zipt-9(tm9416) V</i> ; <i>cdls85</i> [<i>pcc1::2xFYVE::GFP + myo-2p::GFP + unc-119(+)</i>]	This study and CGC, ⁵⁰	FX31843
<i>unc-119(ed3) III</i> ; <i>cdls66</i> [<i>pcc1::GFP::rab-7 + myo-2p::GFP + unc-119(+)</i>]	CGC	NP871
<i>zipt-9(tm9416) V</i> ; <i>cdls66</i> [<i>pcc1::GFP::rab-7 + myo-2p::GFP + unc-119(+)</i>]	This study and CGC	FX31844
<i>unc-119(ed3) III</i> ; <i>pwls50</i> [<i>Imp-1::GFP + Cbr-unc-119(+)</i>]	CGC and ⁴⁹	RT258
<i>zipt-9(tm9416) V</i> ; <i>pwls50</i> [<i>Imp-1::GFP + Cbr-unc-119(+)</i>]	This study and CGC, ⁴⁹	FX31845
<i>pwls72</i> [<i>vha-6p::GFP::rab-5 + Cbr-unc-119(+)</i>] II	This study and CGC, ⁴⁸	FX31846
<i>pwls72</i> [<i>vha-6p::GFP::rab-5 + Cbr-unc-119(+)</i>] II; <i>zipt-9(tm9416) V</i>	This study and CGC, ⁴⁸	FX18670
<i>sid-1(tm2700) V</i>	NBRP	FX16773
<i>sid-1(tm2700) zipt-9(tm9416) V</i>	This study and NBRP	FX18749
<i>sid-2(tm9591) II</i>	This study	FX19710
<i>sid-2(tm9591) II</i> ; <i>zipt-9(tm9416) V</i>	This study	FX18726
<i>sid-2(tm9593) II</i>	This study	FX19716
<i>sid-2(tm9593) II</i> ; <i>zipt-9(tm9416) V</i>	This study	FX19715
<i>sid-3(tm342) X</i>	NBRP	FX19503
<i>zipt-9(tm9416) V</i> ; <i>sid-3(tm342) X</i>	This study and NBRP	FX18738
<i>sid-5(tm4328) X</i>	NBRP	FX19502
<i>zipt-9(tm9416) V</i> ; <i>sid-5(tm4328) X</i>	This study and NBRP	FX18615
<i>sid-5(tm4328) sid-3(tm342) X</i>	This study and NBRP	FX31847
<i>rsd-3(tm9006) sid-3(tm342) X</i>	This study and NBRP	FX31848
<i>sid-5(tm4328) rsd-3(tm9006) X</i>	This study and NBRP	FX31849
<i>sec-22(ok3053) X</i>	This study, CGC, ¹⁶	FX31850
<i>zipt-9(tm9416) V</i> ; <i>sec-22(ok3053) X</i>	This study, CGC, ¹⁶	FX31851
<i>cdf-2(tm788) X</i>	NBRP	FX00788
<i>tmm-1(tm6576) III</i>	NBRP	FX06576
<i>tmm-1(tm6576) III</i> ; <i>cdf-2(tm788) X</i>	This study and NBRP	FX19456
The deletion mutants created using CRISPR/Cas9	See Table S2	

Oligonucleotides

primers used for construction of CRISPR plasmids and genotyping	See Table S3 , Eurofins	
ama-1#F: agatggacctaccgacaac	Eurofins	NA
ama-1#R: ctgcagattacacggaagca	Eurofins	NA
F55C9.3#F: cggaagaaggaaaaccggaatc	Eurofins	NA

(Continued on next page)

Continued

REAGENT or RESOURCE	SOURCE	IDENTIFIER
F55C9.3#R: gcgtctgcggaatgttctct	Eurofins	NA
F55C9.5#F: tccaacaacgacgcaacttta	Eurofins	NA
F55C9.5#R: ggtggcagacaatcaaattct	Eurofins	NA
Recombinant DNA		
pFX_RmT-myo-3(aa1)	This study	NA
Pmtl-1::gfp	This study	pKD228
Pmyo-2::mCherry	Addgene	pCFJ90; RRID:Addgene_19327, https://www.addgene.org/19327/
Pzipt-9::hZIP9	This study	pKD217
Pvha-6::NES::ZapCY2	This study	pKD274
Pvha-6::zipt-9::GFP	This study	pKD156
Pvha-6_zipt-9(H217A)::GFP	This study	pKD235
Pvha-6_zipt-9(H247A)::GFP	This study	pKD264
Pvha-6_zipt-9(H217A, H247A)::GFP	This study	pKD265
Pzipt-9::zipt-9::tagRFP	This study	pKD158
Pzipt-9::zipt-9::EGFP	This study	pKD149
plasmids for CRISPR/Cas9	See Table S4	
Software and algorithms		
ImageJ	Schneider, et al. ⁵¹	SCR_003070
Prism GraphPad 6 for MacOS X	GrapPad Software	

RESOURCE AVAILABILITY

Lead contact

Further information and requests for resources should be directed to and will be fulfilled by the lead contact, Shohei Mitani (mitani.shohei@twmu.ac.jp).

Materials availability

New strains and reagents generated during this project are available through the [lead contact](#).

Data and code availability

- Sequence data generated in the study is available at NCBI BioProject: PRJNA928582. Accession numbers are NCBI Trace Archive: SRR23325556 and NCBI Trace Archive: SRR23325555. Data reported in this paper will be shared by the [lead contact](#) upon request.
- This paper does not report original code.
- Any additional information required to reanalyze the data reported in this paper is available from the [lead contact](#) upon request.

EXPERIMENTAL MODEL AND STUDY PARTICIPANT DETAILS

Bristol N2 was used as wild type strain. Worm cultures, genetic crosses, and other *C. elegans* methods were performed according to standard protocols⁵² except where otherwise indicated. All experiments were performed at 20°C except where otherwise indicated. Detailed information on the strains used is included in the [key resources table](#).

METHOD DETAILS

DNA preparation for injection

Plasmids were prepared using Qiagen's Mini Plasmid Purification Kit (QIAGEN, Hilden, Germany) or PureLink HQ Mini Plasmid kit (Invitrogen, Carlsbad, CA).

Mutagenesis screens

EMS mutagenized F2 progeny of *ccls4251 l*; *rsd-3(tm9006) X*; *tmls961* animals were screened for increased sensitivity to gfp feeding RNAi. Identification of variants in the mutant strains by whole genome sequencing was performed as described previously.^{53,54} Genomic DNA was isolated using a DNeasy Blood & Tissue Kit (Qiagen). A DNA library was prepared from genomic DNA with a LibraryBuilder automatic library synthesis machine (Thermo Fisher Scientific) as described previously. The DNA library was used for the construction of templates by the ionChef system (Thermo Fisher Scientific), and the templates were sequenced to a target depth of approximately 50 using ionProton (Thermo Fisher Scientific) according to the standard protocol. Small variants were identified with variantCaller (<https://github.com/iontorrent/TS/tree/master/plugin/variantCaller>). The whole genome sequence dataset of FX15035: *ccls4251 l*; *rsd-3(tm9006) X*; *tmls961* that was used for EMS mutagenesis was compared to that of the outcrossed suppressor strain FX17549: *ccls4251 l*; *tm9028 V*; *rsd-3(tm9006) X*; *tmls961* (x4 outcrossed with FX15035). Analysis of the G:C to A:T transition for mutant FX17549 showed linkage to chromosome V (Figure S1). FX17549 was further outcrossed with FX15035 twice, and several candidate mutations on chromosome V were tracked by Sanger sequencing. Three deletion mutants for the candidate genes in the outcrossed strain (Table S1) did not show the suppressor phenotype, and we excluded these genes from the candidate causal genes. Then, we focused on *ccz-1*, *ttr-21* and *zipt-9* based on their molecular function and performed rescue experiments using PCR fragments of these genes, which were amplified from N2 genomic DNA. Only the *zipt-9* PCR fragment rescued the suppressor phenotype for RNAi defects in FX17549.

CRISPR/Cas9-mediated genome editing

For generation of deletion mutants for ZnT and ZIP genes, we used the plasmid-based CRISPR/Cas9 method.^{26,27} We used two types of Cas9/sgRNA plasmids: "single-guide Cas9/sgRNA plasmid" containing one U6 promoter::sgRNA, which is structurally identical to pDD162 except for the DNA encoding sgRNA, and "multiguide Cas9/sgRNA plasmid" containing two U6 promoter::sgRNAs.⁵⁵ The Cas9-sgRNA plasmids were made by using a Clontech In-Fusion PCR Cloning Kit (Clontech Laboratories, Palo Alto, CA). We injected a genome editing plasmid mixture containing two single-guide plasmids (50 ng/μl each) or a multiguide Cas9/sgRNA plasmid (100 ng/μl) and an injection marker plasmid pCJ90 (Pmyo-2::mCherry) (10 ng/μl) and an NEB 1 kb DNA ladder (90 ng/μl) into the gonads of wild-type or *rsd-3(tm9006)* animals. Deletions were identified by PCR screening and confirmed by sanger sequencing. The created deletion alleles, the plasmids for CRISPR, and the primers used in plasmid construction and detection of deletion are listed in Tables S3 and S4. The lethal mutations were balanced with balancer chromosomes.^{55,56}

Quantitative PCR

Total RNA from day one adults was manually isolated using TRIzol (Invitrogen). For reverse transcription, Superscript IV reverse transcriptase (Invitrogen) was used following the manufacturer's instructions. Quantitative PCR was performed in a 7500 Real-time Thermal cycler (Applied Biosystems) using the Power SYBR master mix (Applied Biosystems) with the following parameters: 95 °C for 10 min and 40 cycles of 95 °C for 5 s, 55 °C for 10 s and 72 °C for 30 s. Data were normalized to the *ama-1* gene. The primers used are listed in the [key resources table](#).

RNAi by feeding and injection methods in this study was performed as described previously.¹⁴ RNAi clones were transformed into *E. coli* HT115(DE3),⁴⁸ and the bacteria were grown on NGM supplemented with 100 μg/mL ampicillin and 1 mM isopropyl-beta-D-thiogalactopyranoside (IPTG). The RNAi clones for *bli-3*, *unc-15*, *pos-1*, *dpy-13*, *hmr-1*, *lin-1* and *unc-73* were purchased from GeneService and verified by sequencing. The *gfp* RNAi construct used in this study was previously created.¹⁴ To test the effect of supplementation of metal ions on feeding RNAi, dH₂O, ZnSO₄ (at a final concentration of 270 μM), MnCl₂ (at a final concentration of 270 μM), MgSO₄ (at a final concentration of 270 μM) and ferric ammonium citrate (at a final concentration of 6 mg/ml) were added to the NGM plate seeded with HT115 after IPTG induction. These plates were dried for a couple of hours at room temperature, and then the worms were transferred onto them. Data were obtained from several independent experiments. Each experiment included at least 20 animals.

Analysis of *Pmtl-1::gfp*

Zinc sulfate (ZnSO₄·7H₂O, Wako 268-00405) was dissolved in water and autoclaved to make a 1 M stock solution. The stock solution was subsequently diluted 1:100 (10 mM) with sterilized water and added to

molten Noble agar medium before preparing individual plates. Approximately 50 transgenic L4 hermaphrodites (wild type, *zip1-9(tm9416)* and *rsd-3(tm9006)*) expressing GFP under the control of the *mtl-1* promoter (*tmEx4662[Pmtl-1::gfp]*) were transferred to Noble agar plates with ZnSO₄ (0, 1, 5, and 10 μM) and incubated at 20 °C for 24 h. Then, animals were imaged under a BX-51 microscope (Olympus).

Analysis of FRET-based Zn²⁺ sensor ZapCY2

A 10 mM ZnSO₄ solution was directly added to an OP50-seeded NGM agar plate (final concentration of 270 μM ZnSO₄). Approximately 50 transgenic day 1 adult hermaphrodites (wild type, *zip1-9(tm9416)* and *rsd-3(tm9006)*) expressing the FRET sensor under the control of the intestine specific *vha-6* promoter (*tmEx4758[Pvha-6::NES-ZapCY2]*) were transferred to OP50-seeded NGM agar plates with ZnSO₄ and incubated at 20 °C for the indicated time period. Animals were imaged under a BX-51 microscope (Olympus).

Imaging

Animals expressing fluorescent proteins were mounted on 5% agar pads and imaged with a BX51 microscope equipped with a DP80 CCD camera (Olympus Optical Co., Ltd) or Carl Zeiss LSM710. To estimate colocalization between channels (Figure 4G), Pearson's coefficient between channels was quantified by the plug-in Coloc2 in Fiji. To quantify cytosolic Zn²⁺ levels, the posterior intestine was excited at 438 nm, and the FRET ratio was calculated by dividing the intensity of the YFP signal (filtered by Semrock: FF01-542/27-25) by the CFP signal (filtered by Semrock: FF01-483/32-25) by using the RatioPlus plug-in of ImageJ.²⁹

QUANTIFICATION AND STATISTICAL ANALYSIS

Data were presented as mean ± SEM. Statistical analysis for all data was carried out using Student's t-test (unpaired, two-tailed) or ANOVA followed by Tukey's post-hoc test. Statistical analysis was performed using Prism 6 software.